Natural Resources Canada / Ressources naturelles Canada

GEOLOGICAL SURVEY OF CANADA
OPEN FILE 8121

Shear Wave Velocity Estimation from Piezocone Test Data for Eastern Canada Sands (Quebec and Ontario) – Extended Version with Appendices

D. Perret, E. Charrois, M. Bolduc

2016

Celebrating 175 yrs

Canada

GEOLOGICAL SURVEY OF CANADA
OPEN FILE 8121

Shear Wave Velocity Estimation from Piezocone Test Data for Eastern Canada Sands (Quebec and Ontario) – Extended Version with Appendices

D. Perret[1], E. Charrois[2], M. Bolduc[3]

[1] Natural Resources Canada
[2] Englobe Corp., Québec, Québec
[3] Ministère des Transports, de la Mobilité Durable et de l'Électrification, Québec, Québec

2016

doi:10.4095/299413

This publication is available for free download through GEOSCAN (http://geoscan.nrcan.gc.ca/).

Recommended citation
Perret, D., Charrois, E., Bolduc, M., 2016. Shear wave velocity estimation from piezocone test data for Eastern Canada sands (Quebec and Ontario) – Extended version with appendices; Geological Survey of Canada, Open File 8121, 47 p. doi:10.4095/299413

Publications in this series have not been edited; they are released as submitted by the author.

Contents

List of Figures

Abstract

Different relations between shear wave velocity and parameters obtained from seismic cone penetration tests are evaluated against a data set collected at 107 sites along the St. Lawrence River Valley in Eastern Canada. Only sands or sand-like soils with a normalized SBT index I_c less than 2.60 and a normalized porewater pressure ratio B_q less than 0.10 are considered in this study. All investigated soils are approximately 7,000-12,000 years old and are of a marine, mainly deltaic, origin. Correlations established for Holocene sands systematically under-predict shear wave velocities determined for the tested soils while the opposite is observed for correlation developed for Pleistocene sands. Non-linear regressions and residual analyses conducted for the tested soils indicate that the best prediction model has a functional form incorporating the cone tip resistance, the sleeve friction resistance, and the effective vertical overburden stress. A good correlation is also obtained with only the cone tip resistance and depth. As a result, two new equations are presented specifically for sands in the St. Lawrence River Lowlands which allow for an estimation of shear wave velocity based on piezocone test data. This open-file report is an extended version of a paper presented at the 69$^{\text{th}}$ Canadian Geotechnical Conference in Vancouver (Perret et al., 2016).

Résumé

Différentes relations entre la vitesse de propagation des ondes de cisaillement et les paramètres obtenus lors d'essais au piézocône sismique sont évaluées pour des données collectées à 107 sites répartis le long de la vallée du St-Laurent dans l'est du Canada. Seuls les sables, caractérisés par un indice SBT normalisé I_c inférieur à 2.60 et un rapport normalisé de pression interstitielle B_q inférieur à 0.10, sont retenus. Tous les sables testés ont un âge compris entre 7,000 et 12,000 ans environ, et sont d'origine marine, principalement deltaïque. Les relations établies pour les sables d'âge holocène sous-prédisent systématiquement les vitesses des ondes de cisaillement, tandis que l'opposé est observé pour les sables d'âge pléisotocène. Les régressions non-linéaires et l'analyse des résidus effectuées pour les sables testés montrent que le modèle ayant le meilleur pouvoir prédictif a une forme fonctionelle incorporant la résistance en pointe, la friction développée le long du manchon, et la contrainte effective verticale due aux poids des terres. Une bonne corrélation est également obtenue en considérant simplement la résistance en pointe et la profondeur. Nous proposons donc deux nouvelles équations, établies spécifiquement pour les sables des basses terres de la vallée du St-Laurent, permettant d'estimer les vitesses de propagation des ondes de cisaillement à partir de données obtenues à l'aide d'essais au piézocône. Ce dossier public est une version allongée d'un article présenté lors de la 69$^{\text{th}}$ Conférence canadienne de géotechnique à Vancouver (Perret et al., 2016)

.

1 Introduction

Shear wave velocity is a fundamental parameter for analyzing soil behaviour under both static and dynamic loading and is consequently used in a broad spectrum of applications (Clayton, 2011). For example, this parameter is required in most constitutive models to evaluate the small strain response of soils, may be used to estimate the in-situ stress state of cohesionless soils (Cunning et al., 1995), and, as the level of amplification of ground motions generated during an earthquake depends on the stiffness of soil layers, it serves as a basis for seismic site classification in many design codes, including the current National Building Code of Canada and the Canadian Highway Bridge Design Code. Shear wave velocity appears also to be a critical parameter in assessing the potential for liquefaction triggering of cohesionless soils (Andrus et al., 2004; Dobry and Abdoun, 2015).

Different in-situ techniques are available for determining shear wave velocities in the near surface (Hunter and Crow, 2012). Non-invasive tests like seismic reflection, SASW, or MASW are relatively inexpensive to carry out but data processing and interpretation are sometimes challenging, and the resulting velocity profiles may not always have the appropriate resolution and accuracy for geotechnical applications. Amongst invasive techniques, the seismic piezocone test (or seismic cone penetration test with pore pressure measurements, SCPTu) is probably the best tool to obtain, at reasonable cost, detailed and reliable shear waves velocity profiles in soils ranging from clays to coarse sands. The coupling between the probe and the surrounding soil is excellent and, by taking care of correctly isolating the push rods from ambient vibrations during the test, identification of shear wave propagation times in records is usually straightforward and accurate. Another obvious advantage of using a SCPTu probe is that continuous profiles of cone tip resistance, sleeve friction resistance, and pore pressure, are generated, allowing the identification of site stratigraphy and the establishment of correlations between these parameters and shear wave velocities determined during the same penetration test.

The purpose of this report is first to review, for sand deposits located in Eastern Canada along the St. Lawrence River Valley and its tributaries, the suitability of some commonly used correlations proposed in the literature between shear wave velocity (Vs) and CPTu parameters, and then to define new correlations tailored to these sands. Such correlations will allow for improved estimates of V_s using available CPTu databases in Eastern Canada for application in low risk projects, or to produce regional maps of seismic ground motions. They will also allow for verification of anomalous V_s values measured from SCPTu, or with other geophysical techniques, if conventional CPTu data are available.

2 Factors influencing shear wave velocity and piezocone test parameters in sands

Theoretical considerations based on micromechanical analyzes of particle interaction indicate that the overall shear modulus (and thus shear wave velocity) in non cemented granular materials is a function of particle packing, particle Poisson's ratio and shear modulus, and state of stress (e.g. Petrakis and Dobry, 1987; Santamarina and Cascante, 1996). Dependency on these factors has been corroborated in multiple experimental studies and it is now well established that the shear modulus G_0 of cohesionless soils can be expressed semi-empirically as:

$$G_0 = \rho\, V_s{}^2 = A\, F(e)\, \sigma_x'^{\,n}\, \sigma_y'^{\,m}\, p_a^{1-n-m} \tag{1}$$

where ρ is the soil mass density, V_s, the shear wave velocity, A, a dimensionless coefficient accounting for possible structural aging effects like cementation or fabric rearrangement, $F(e)$, a function of the void ratio e, σ_x', the effective stress acting in the direction of shear wave propagation, σ_y', the effective stress acting in the direction of particle motion, n and m, two stress exponents which are typically equal to ≈ 0.25, and p_a, a reference stress usually taken as the atmospheric pressure in the same unit as σ_x' and σ_y'. In a seismic piezocone test, the direction of wave propagation is essentially vertical while the direction of particle motion is horizontal.

Unlike the small strains induced from shear waves created with typical impact sources used in geotechnical site characterization, pushing a CPT probe into the ground induces very large strains. Despite a mismatch in strain levels that can cover more than five orders of magnitude, the cone tip resistance is influenced by several factors controlling shear wave velocity, as shown for example by Houlsby and Wroth (1989), Lunne et al. (1997), Salgado et al. (1997), Schnaid and Yu (2007), and Salgado (2014). According to experimental evidence and theories based on bearing capacity, cavity expansion or on steady state deformation, these factors are: the void ratio, through the relative density or the state parameter; the effective stress state with a predominant effect of the horizontal effective stress; and to a lesser extent the structure of the sand, with reduced effects at very large strains. In addition, the cone tip resistance depends on intrinsic variables of the sand, such as the critical-state friction angle and compressibility, and on the soil stiffness.

Factors influencing the sleeve friction resistance are mainly related to the radial effective stress field around the sleeve where the sand is brought to a plastic state, to the friction between soil and sleeve surface, and possibly to the structure of the sand at shallow depths (Puppala et al., 1995) even if strains are large. It is important to highlight, as it may have an influence in establishing correlations and on data dispersion, that the measurement of the sleeve friction resistance is known to be highly variable and less reliable than the cone tip resistance measurement (Lunne et al., 1997).

At a standard penetration rate of 2 cm/s the penetration test is essentially a drained test due to the high hydraulic conductivity of sands. Pore pressures generated by the cone penetration at or near the cone tip dissipate very quickly and the measured pore pressures are thus usually close or equal to the in-situ natural equilibrium (pre-test) pore pressures.

This brief overview suggests that the most dominant factors that should be considered in correlations with shear wave velocity are the cone tip resistance, possibly the sleeve friction resistance, and aging effects. The stress state should also be considered as shear wave velocity and piezocone test parameters strongly depend on it. In practice, however, the horizontal effective stress is generally unknown due to great difficulties in determining this parameter with a reasonable accuracy, and only the effective vertical stress or depth can be realistically used as a proxy in correlations. As some factors, like critical state parameters, influence piezocone parameters but not shear wave velocity, only moderately good correlations can be expected between variables.

3 Geological setting of SCPTu sites

The 107 sites examined in this study were selected to ensure a representative sampling of sand deposits along the St. Lawrence River Valley and tributaries, where most of the population is concentrated (Fig. 1). Sands were deposited in marine, mainly deltaic, environments, during late Pleistocene and early Holocene, approximately between 12,000 to 7,000 years ago.

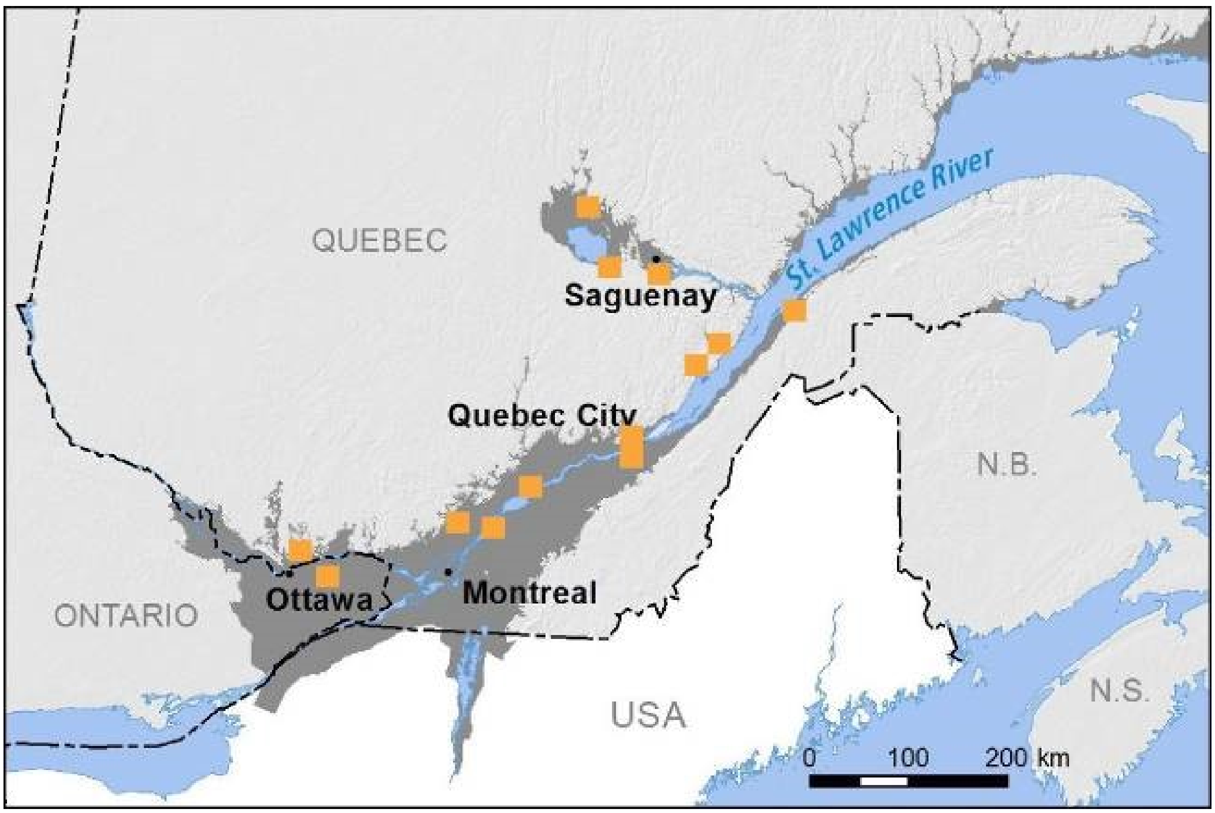

Figure 1 – Location of seismic piezocone test areas (an orange square can represent several sites). Dark grey areas show the extent of late Pleistocene and early Holocene marine deposits.

Even though sites are distributed along a stretch of the St. Lawrence River Valley more than 500 km long, the physical properties of these sands (particle angularity and mineralogy) are relatively homogeneous as they were transported in glaciofluvial or postglacial fluvial streams over similar distances and originate from the glacial abrasion of the same Canadian shield rocks, principally plutonic and high grade metamorphic rocks. This geological consistency implies that unique empirical correlations can be reasonably proposed for the entire area, from the Ottawa region to the Saguenay region.

4 Methods of analysis

4.1 Seismic piezocone tests

4.1.1 Data processing

Piezocone tests were conducted according to the ASTM D5778-12 (ASTM, 2012) with probes equipped with compression-type tip and sleeve load cells. Porewater pressure were measured just behind the cone in a u_2 position. A particular attention was paid to ensure a full saturation of the porous element and porewater sensor chamber in order to correctly detect sand/clay or clay/sand layering. For shear wave velocity measurements, seismic signals were recorded at 1 m depth intervals at each site, in two opposite polarities. The horizontal offset between the shear wave source and the piezocone rods was between 0.5 and 1.5 m depending on the pushing equipment. Differential shear wave propagation times were determined from two consecutive traces by manually picking times either at same phase points (first main trough or peak) or at first cross-over points, but in a consistent manner for a given profile. To avoid having unrealistically irregular velocity profiles due to small errors made in picking times, propagation time profiles were lightly smoothed with a second order Savitzky-Golay filter with a frame size of 3 to 7 data points (Schafer, 2011). Shear wave velocities were calculated with the pseudo-interval method. Several comparative analyses showed that differences with velocities obtained with the more accurate Snell's law ray path method (Kim et al., 2005) are insignificant for the small offsets used.

Total and effective stress profiles, and CPTu data profiles were discretized into 1 m long segments to correspond to shear wave velocity profiles (Fig. 2). Median values of each variable were calculated for 1 m segments and assigned to the midpoint of each segment. The median was preferred over the arithmetic mean as the median is less sensitive to extreme values.

4.1.2 Identification of cohesionless soils

Identification of cohesionless soils was based on the normalized Soil Behavior Type (SBTn) index I_c and the normalized porewater pressure ratio B_q. The rationale supporting the use of these parameters is presented e.g. in Jefferies and Davis (1993), Mayne (2007), Robertson (2009), and Robertson and Cabal (2015). The SBTn index I_c is calculated according to Robertson (2009):

$$\mathrm{I}_c = \left[\left(3.47\ \log \mathrm{Q}_{tn}\right)^2 + \left(\log \mathrm{F} + 1.22\right)^2\right]^{0.5} \tag{2a}$$

where Q_{tn} is the normalized cone penetration resistance:

$$\mathrm{Q}_{tn} = \left(\frac{q_t - \sigma_{v0}}{p_a}\right)\left(\frac{p_a}{\sigma'_{v0}}\right)^n \tag{2b}$$

and F is the normalized sleeve friction resistance ratio, in %:

$$\mathrm{F} = 100\ \frac{f_s}{q_t - \sigma_{v0}} \tag{2c}$$

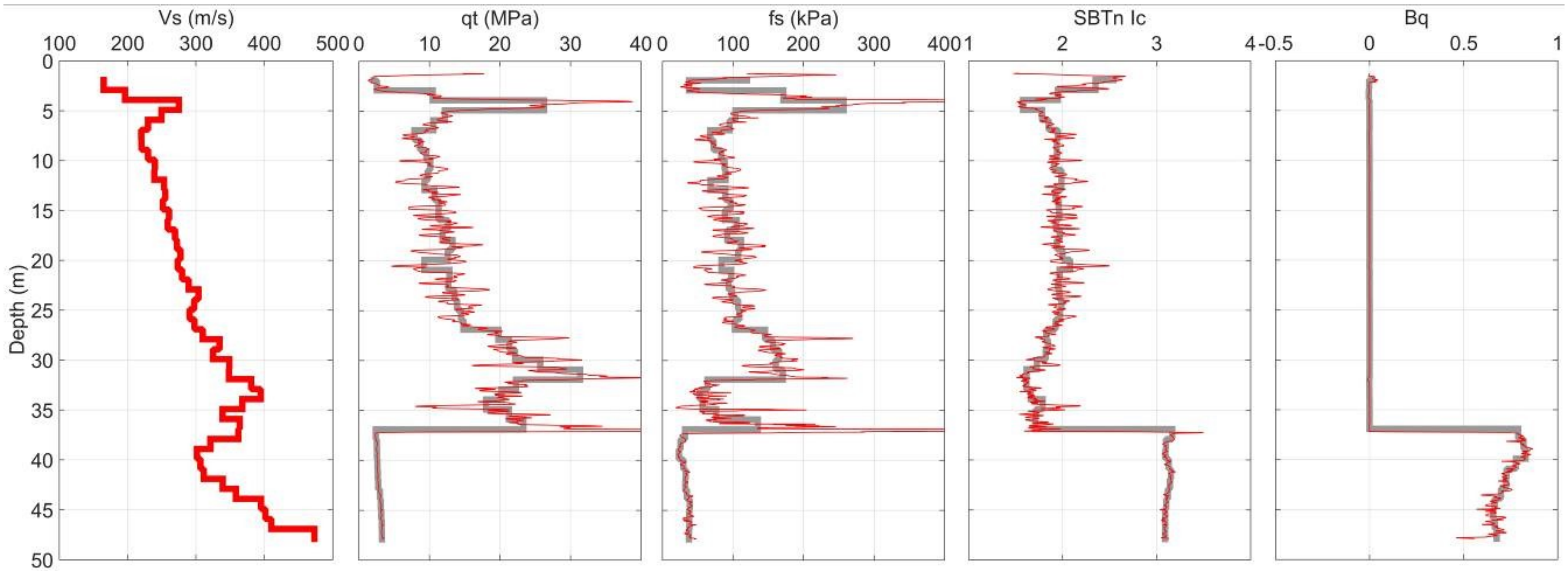

Figure 2 – Example of discretization at 1 m depth intervals of seismic piezocone test profiles for a site in Quebec City. Dark grey staircase profiles correspond to discretized profiles. Vs is the shear wave velocity, q_t, the corrected cone tip resistance, f_s the sleeve friction resistance, SBTn I_c, the normalized Soil Behavior Type Index, and B_q, the normalized porewater pressure ratio.

where q_t is the cone penetration resistance corrected for porewater effects, σ_{v0}, the total vertical overburden stress, σ'_{v0}, the effective vertical overburden stress, p_a, the atmospheric pressure, and f_s, the sleeve friction resistance. The variable stress exponent n is a function of the SBTn index I_c and vertical effective overburden stress, and is calculated iteratively until change in n is ≤ 0.01:

$$n = 0.381\, I_c + 0.05\, \frac{\sigma'_{v0}}{p_a} - 0.15 \tag{2d}$$

The normalized porewater pressure ratio B_q is defined as:

$$B_q = \frac{u_2 - u_0}{q_t - \sigma_{v0}} \tag{3}$$

where u_2 is the porewater pressure generated by cone penetration, and u_0 is the in-situ equilibrium porewater pressure. The soil unit weights were assumed in calculations to be 17.5 and 19.0 kN/m^3, respectively above and below the groundwater table (e.g. Andrus et al., 2007).

In this study, soils characterized by both $I_c \leq 2.60$ and $B_q \leq 0.10$ are considered cohesionless. According to the normalized SBTn classification (Robertson, 2009; Robertson and Cabal, 2015), soils with $I_c \leq 2.60$ range from sand mixtures (sandy silts or silty sands) to coarse sands, with the following thresholds:

- $I_c \leq 1.31$: gravelly sands to dense sands
- $1.31 < I_c \leq 2.05$: clean sands to silty sands
- $2.05 < I_c \leq 2.60$: silty sands to sandy silts.

The range $2.50 \leq I_c < 2.70$ represents a transition in soil behaviour, from soils having a predominantly sand-like to a predominantly clay-like behaviour. The second threshold on B_q is aimed at ensuring that soils having a clay-like behaviour are effectively excluded (Mayne, 2007). In total, 1258 pairs of shear wave velocities and CPTu data meeting these two I_c and B_q criteria were formed.

As pointed out by Robertson (2009), the SBTn index I_c cannot be expected to provide a classification of soil types exactly equivalent to classifications directly based on physical characteristics of soils. Although there is generally a good agreement between the Robertson's (2009) classification based on CPT parameters and classifications based on soil physical properties, it is important to check the dependency of I_c on the physical nature of the tested soils, and thus the validity of the threshold used to identify cohesionless soils.

The following two figures (Figs 3 and 4) show I_c as a function of the fines content and the median grain-size diameter D_{50} for soil samples retrieved at a few piezocone test sites. For comparison purposes, data compiled by Andrus et al. (2004, 2007) are also presented. Scatter in the data is large but to a level comparable with Andrus' data. In Fig. 3, I_c increases as expected with the amount of fines, following the trend observed by Boulanger and Idriss (2016). Except for a few outliers, data points are located within a range of $\pm 1\sigma$ with respect to the average relation of Boulanger and Idriss for I_c lower than 2.60 (as shown by the dashed red line).

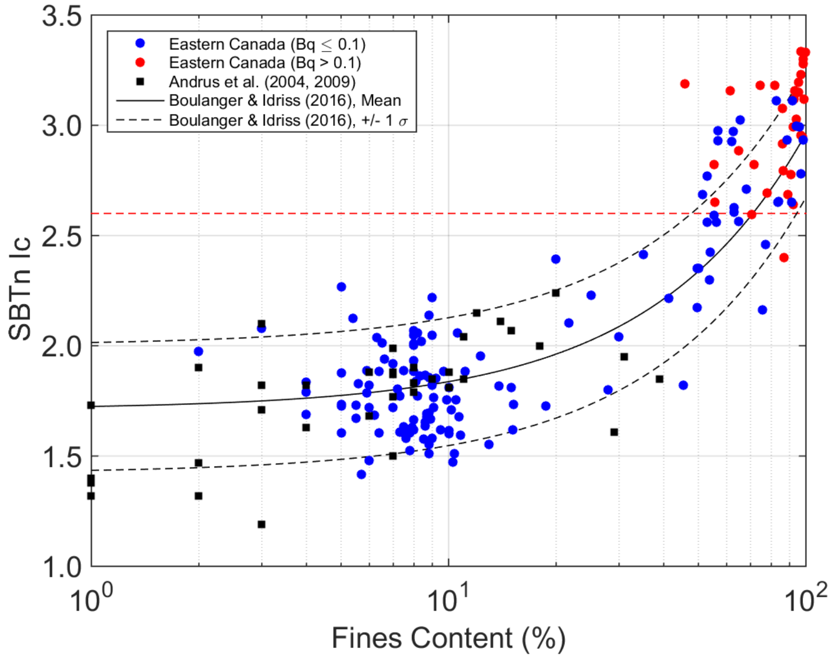

Figure 3 – Normalized soil behaviour type index I_c as a function of fines content for some soils investigated in this study and differentiated according to the normalized porewater pressure ratio B_q. Data compiled by Andrus et al. (2004, 2009) are presented for comparison purposes.

Data points are differentiated in Fig. 3 according to the threshold applied on the normalized porewater pressure ratio ($B_q \leq 0.10$). Only two data points with $B_q > 0.10$ are under the line $I_c = 2.60$ and the usefulness of applying a second filter based on B_q may be questioned. However, soil samples for which grain-size analyzes were available represent a small subset of the whole seismic piezocone data set and it is possible that soils characterized by $I_c \leq 2.60$ and $B_q > 0.10$ are in fact more frequent. It was thus judged appropriate to maintain this threshold on B_q. It is also interesting to note that several data points with $B_q \leq 0.10$ are above the line $I_c = 2.60$. These data points correspond to relatively poorly sorted overconsolidated soils, possibly marine diamictons, mainly encountered in the Quebec City region.

Similar comments can be made for Fig. 4. For $I_c \leq 2.60$, I_c decreases with an increase in soil coarseness, with average D_{50} corresponding to grain-size classes ranging from silt to medium/coarse sand. The best fit equation for the filtered data set is:

$$I_c = 1.484\ D_{50}^{-0.181} \tag{4}$$

with a standard deviation of the model prediction error $\sigma = 0.21$.

Fig. 5 presents I_c as a function of D_{50}, as in Fig. 4, but data points are differentiated according to a plasticity index cut-off, instead of a cut-off on the normalized porewater pressure ratio B_q. The cut-off value was chosen based on Fig. 15 presented in Boulanger and Idriss (2006). Soils with a plasticity index lower than 3 may contain a fair amount of fines but have a sand-like behaviour, and can be considered non-plastic and cohesionless. For the soil samples analyzed, all data points with $I_c \leq 2.60$ and $B_q \leq 0.10$ correspond to soils with a plasticity index lower than 3, and are thus cohesionless. Consequently, and with the caution that the number of samples analyzed is small compared to the whole seismic piezocone data set, the physical nature of soils in the filtered data set appears to be in very good agreement with the SBTn classification.

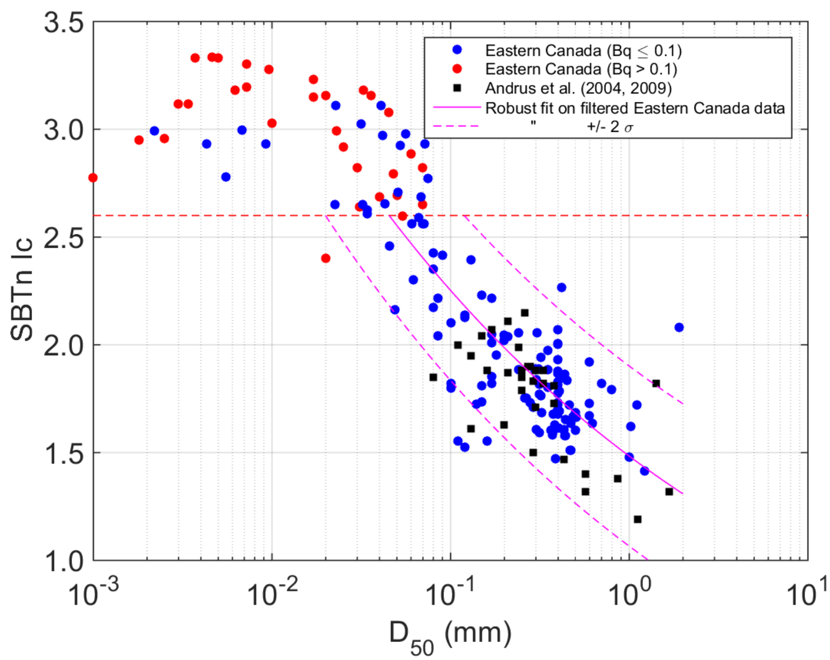

Figure 4 – Normalized soil behaviour type index I_c as a function of D_{50} for some soils investigated in this study and differentiated according to the normalized porewater pressure ratio B_q. Data compiled by Andrus et al. (2004, 2009) are presented for comparison purposes.

4.2 Statistical regressions

Proposing correlations suitable to Eastern Canada sands and sand-like soils requires a function linking the dependent variable, the shear wave velocity, to the predictor variables obtained from CPTu data and possible additional variables like the effective overburden pressure or depth.

Numerous empirical analyses presented in the literature suggest that a simple multiplicative combination of power functions of predictor variables captures much of the variability since they are nonlinearly related to each other (see Wair et al., 2012, and McGann et al., 2015a, for a review). This type of functional form is partly supported by the theoretical approach followed by Schnaid and Yu (2007), and is used here. We did not try to use more complicated functional forms in the absence of a more comprehensive theoretical basis.

Multivariate nonlinear regressions were run in Matlab® with the function *fitnlm* available in the Sta-

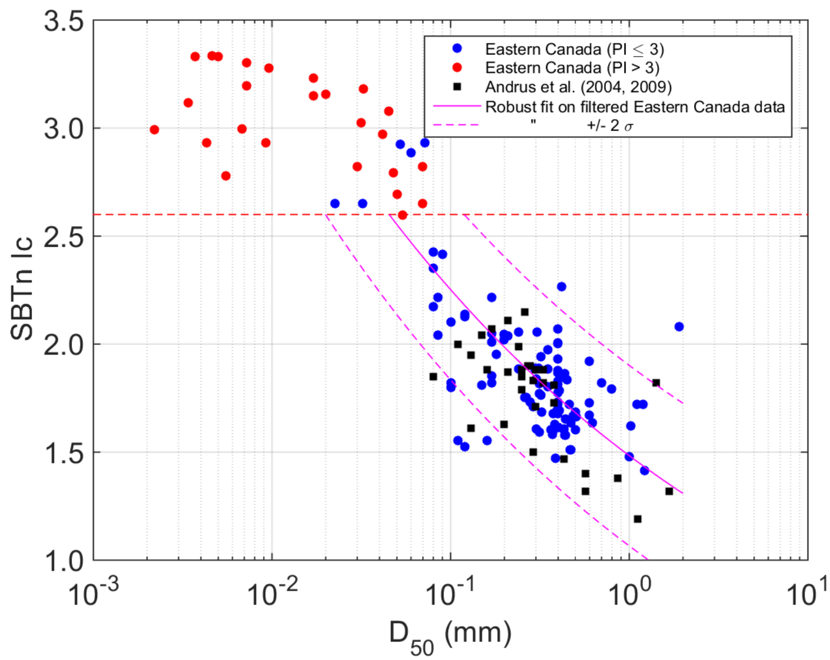

Figure 5 – Normalized soil behaviour type index I_c as a function of D_{50} for some soils investigated in this study and differentiated according to the plasticity index PI. Data compiled by Andrus et al. (2004, 2009) are presented for comparison purposes.

tistical toolbox. Functional forms were not transformed to linear models by taking logarithms of the function components, as often done, due to statistical considerations on the log-normality of the error term distribution. Also, it was preferred to not use regression equations with one or more identical variables (hidden or explicit) on both sides of an equation to avoid possible spurious correlation effects that may artificially enhance statistical link between the dependent and predictor variables.

The agreement of regression models to the data set was evaluated in accordance with the concepts of exploratory data analysis (EDA; e.g. Chambers et al., 1983; NIST, 2012), which combines a quantitative description and a visual appraisal of the goodness of fit. Residuals, defined here as the standardized difference between the measured and predicted shear wave velocities, were analysed to better detect bias in models.

5 Results

5.1 Distribution of data

Fig. 6 shows depth profiles for the seismic piezocone data set filtered with $I_c \leq 2.60$ and $B_q \leq 0.10$ to retain only cohesionless soils. Each point corresponds to the median value of parameters assigned to the midpoint of 1 m depth intervals, as explained in section 4.1. Points with normalized SBTn I_c values higher than 2.05 are mainly concentrated at the lower bound of shear wave velocity and cone tip resistance data clouds, which may reflect the influence of an increase in fines content. For the sleeve friction resistance, high I_c values are more dispersed and no trend can be evidenced. Although about only 1% of data were obtained at depths between 35 m and 47 m, the whole filtered data set is considered to cover as wide a depth range as possible.

The scatter plot matrix in Fig. 7 displays the relationships for all pairing of filtered variables considered in this study (V_s, q_t, f_s, I_c, σ'_{v0}, and z). Plots along the matrix diagonal also show the data range and histogram for each variable. The weakest relationships, at least visually, are observed between I_c and V_s, I_c and z, and I_c and σ'_{v0}. The vertical effective overburden pressure, σ'_{v0}, appears to be a better predictor than depth z, irrespective of the paired variable.

5.2 Agreement between the filtered data set and some commonly used regression equations

Six published correlations commonly used in engineering practice in Eastern Canada are compared with the filtered data set. The results are presented in Fig. 8 to graphically assess the goodness of fit (NIST, 2012). For each correlation, four plots, noted a, b, c and d, are presented, showing:

(a) The predicted shear wave velocity as a function of the measured shear wave velocity. For a perfect fit, data points are aligned along the 1:1 diagonal (in red). Data points are coloured according to their local density in the plot (Eilers and Goeman, 2004; Henson, 2013), from deep blue (low density) to dark red (high density). This type of display permits to better identify possible bias and to easily determine areas where values are concentrated.

(b) A normal probability plot in which residuals are plotted against a theoretical normal distribution. Normally distributed residuals fall along a straight line (in red), with a slope reflecting the dispersion around the mean value of residuals. If dispersion is purely due to random processes, a normal distribution is expected.

(c) The predicted shear wave velocity as a function of the standardized residuals. Ideally, data points should be centred around a null residual throughout the range of fitted values, and no trend or drift should be detected in the data cloud.

(d) A histogram showing the distribution of residuals also identifies skewness in the distribution, outliers, etc. The best fit curve to residuals is shown in red for a normal distribution.

These four plots show the same data for a given correlation but presented differently to highlight subtleties in the goodness of fit that can be harder to appreciate with only one plot. Results of the six correlations are now briefly presented and commented below.

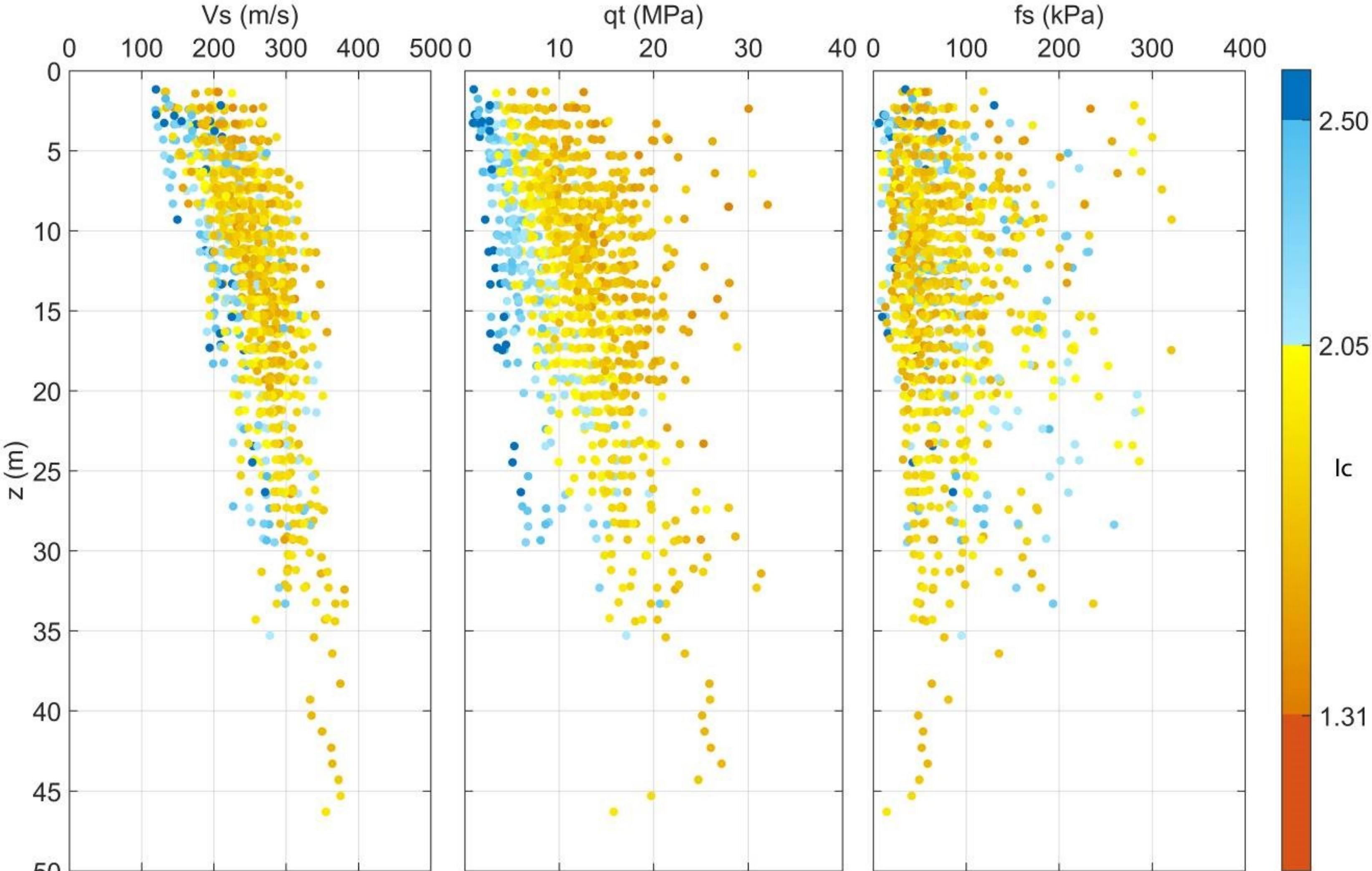

Figure 6 – Depth profiles for shear wave velocity (Vs), corrected cone tip resistance (q_t), and sleeve friction resistance (f_s). The data set is filtered to retain cohesionless soils with SBTn $I_c \leq 2.60$ and $B_q \leq 0.10$. The I_c scale on the right extends from 1.00 to 2.60.

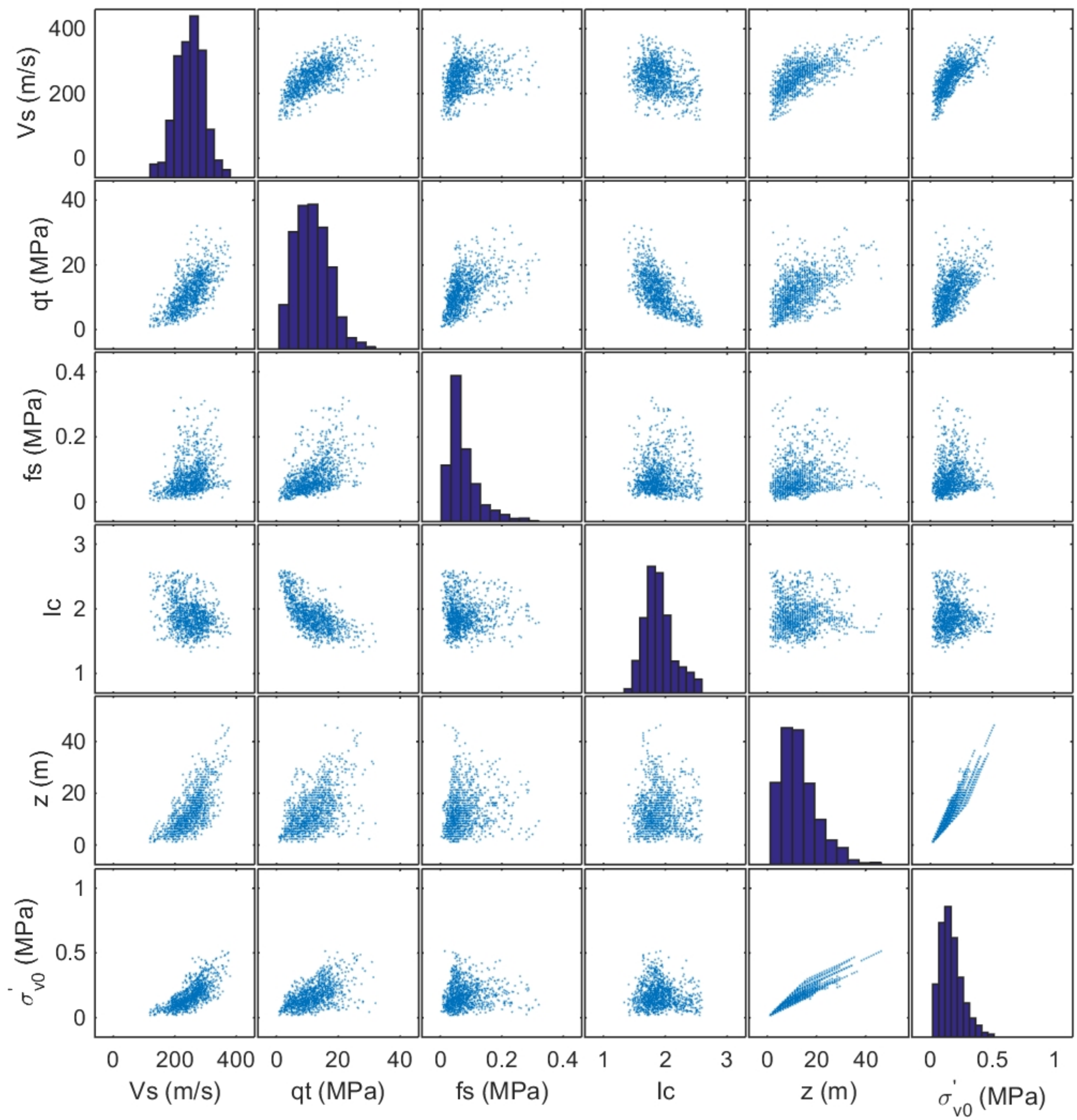

Figure 7 – Scatter plot matrix for pairs of filtered variables considered in this study. Plots along the diagonal show the histogram for each variable.

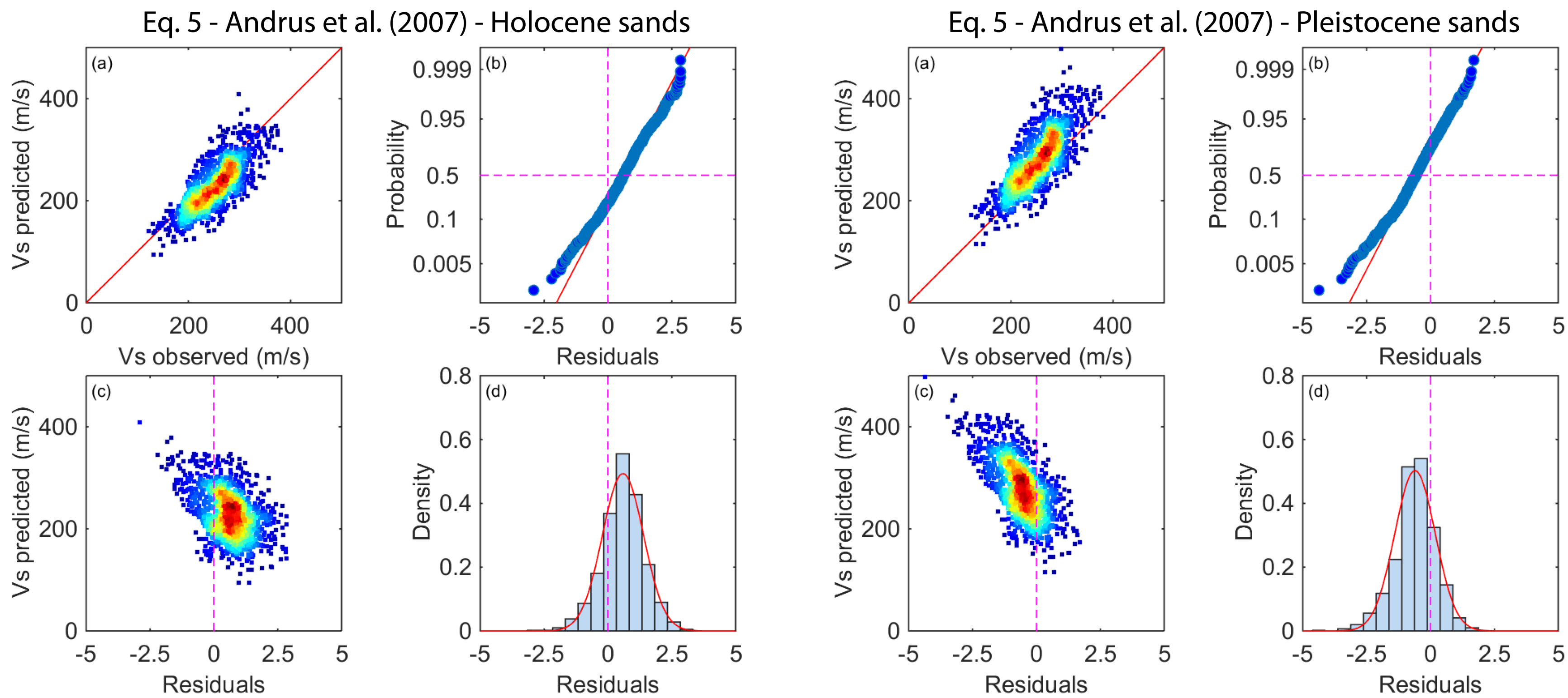

8A

Figure 8 – Plots showing the goodness of fit for six correlations used in Eastern Canada for cohesionless soils.

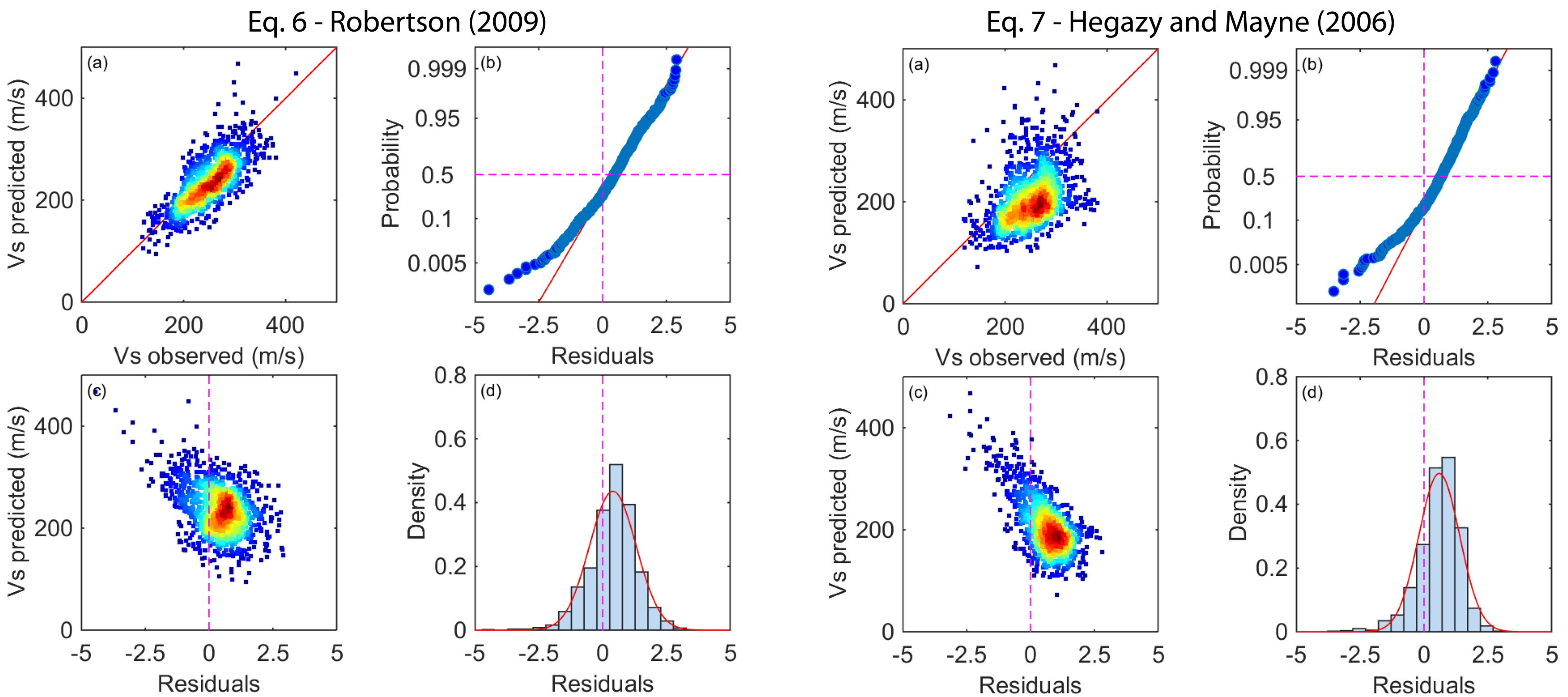
Eq. 6 - Robertson (2009)
Eq. 7 - Hegazy and Mayne (2006)
(a)
(b)
(c)
(d)
Vs predicted (m/s)
Vs observed (m/s)
Probability
Residuals
Density
0.999
0.95
0.5
0.1
0.005
0
200
400
-5
-2.5
0
2.5
5
0.2
0.4
0.6
0.8

8B – cont.

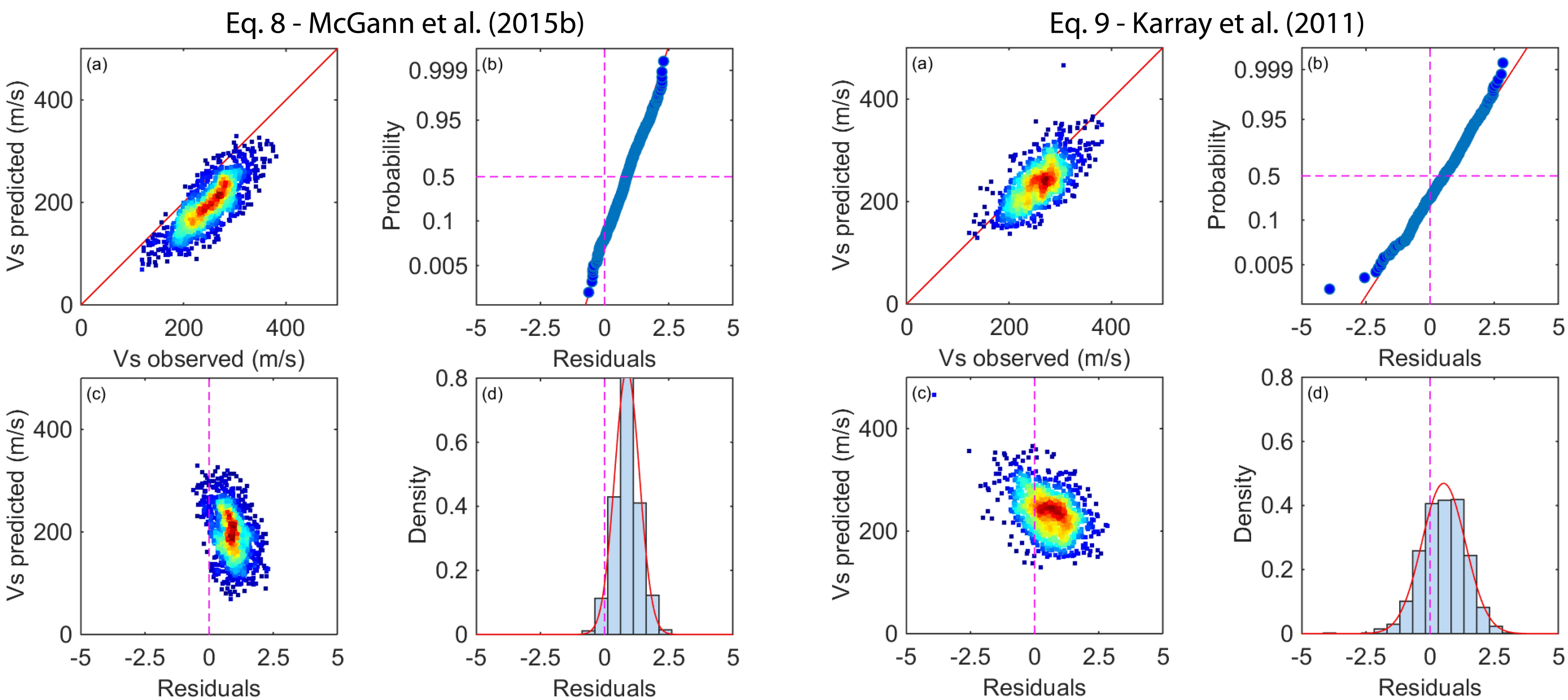
Eq. 8 - McGann et al. (2015b)
Eq. 9 - Karray et al. (2011)
(a)
(b)
(c)
(d)
Vs predicted (m/s)
Vs observed (m/s)
Probability
Density
Residuals
0.999
0.95
0.5
0.1
0.005
0
200
400
-5
-2.5
0
2.5
5
0.2
0.4
0.6
0.8

8C – cont.

5.2.1 Andrus et al. (2007) correlations

These authors developed regression equations considering both soil types and geologic age based on data from California, South Carolina, and Japan. For sands, the recommended regression equation is:

$$V_s = 2.62\ {q_t}^{0.395}\ {I_c}^{0.912}\ z^{0.124}\ \mathrm{SF} \tag{5}$$

where the shear wave velocity V_s is in m/s, q_t, the corrected cone tip resistance in kPa, I_c, the unitless normalized SBTn index, z, the depth below the ground surface in m, and SF, a scaling factor equal to 0.92 or 1.12, respectively for Holocene (< 10,000 years) and Pleistocene (10,000 to 1.8 million years) sands. Most data were acquired at depths less than 20 m.

5.2.2 Robertson (2009) correlation

The regression equation is established for mostly uncemented Holocene and Pleistocene soils, originating from California and other non specified regions:

$$V_s = \sqrt{10^{\ (0.55\ I_c\ +1.68)}\ \frac{q_t - \sigma_{v0}}{p_a}} \tag{6}$$

where σ_{v0} is the vertical overburden stress in kPa, p_a , the atmospheric pressure in kPa, and other terms are as previously defined. The maximum overburden stress at which data were obtained is 580 kPa, which corresponds to a depth of about 60-70 m depending on the unit weight considered.

5.2.3 Hegazy and Mayne (2006) correlation

The correlation is based on a compilation of different soil types, including sands, clays, soil mixtures, and mine tailing materials, from different regions and geological environments in the USA, Japan, and Italy. The regression equation, developed with normalized variables, is presented here in terms of Vs:

$$V_s = 0.0831\ q_{c1\mathrm{N}} \left(\frac{\sigma'_{v0}}{p_a}\right)^{0.25}\ e^{\ 1.786\ I_c} \tag{7}$$

where σ'_{v0} is the effective vertical overburden stress in kPa, $q_{c1\mathrm{N}}$, the normalized raw cone tip resistance, e, the Euler's constant, and other terms are as previously defined.

5.2.4 McGann et al. (2015b) correlation

This new regression equation has been specifically developed for Holocene sands in the Christchurch area in New-Zealand. Sands were deposited in a variety of environments (fluvial, estuarine, coastal, lagoonal, eolian). The best fit equation is:

$$V_s = 18.4\ {q_c}^{0.144}\ {f_s}^{0.0832}\ z^{0.278} \tag{8}$$

where q_c is the raw cone tip resistance, f_s, the sleeve friction ratio, and z, the depth. The majority of piezocone test data were obtained at depths less than 16 m and the regression is valid for $I_c \leq 2.60$.

5.2.5 Karray et al. (2011) correlation

Soils considered in establishing this regression equation are uncemented glaciofluvial sands deposited in the Lake Saint-Jean–Saguenay region in Quebec (Fig. 1), between 7,800 and 9,800 years ago. The equation (Eq. 15 in Karray et al., 2011) is expressed in normalized variables and is a function of the median grain size diameter D_{50}. Replacement of D_{50} with I_c according to Eq. 13 of their paper, and subsequent term rearrangement, produces equation 9 in terms of V_s:

$$V_s = 36.9\, {q_{c1}}^{0.25}\, {I_c}^{-0.958} \left(\frac{\sigma'_{v0}}{p_a}\right)^{0.25} \tag{9}$$

where q_{c1} is the overburden-corrected raw cone tip resistance in kPa, and other variables are as previously defined. The maximum depth at which data were acquired is about 40 m. The validity of the initial correlation based on D_{50} (Eq. 15) is restricted to $0.2 \le D_{50} \le 10$ mm, while Eq. 13 is valid for $I_c \le 2.60$. To stay within the range recommended by Karray et al. (2011), Fig. 8C (right panel) was generated with $I_c = 2.05$, this value being obtained from Eq. 13 for $D_{50} = 0.2$ mm.

5.2.6 General comments

Fig. 8 shows that these six regression equations predict shear wave velocities with significant bias from piezocone test data for Eastern Canada sands. Except for the correlation developed by Andrus et al. (2007) for Pleistocene sands, all equations tend, on average, to severely underestimate shear wave velocities. The equation by Karray et al. (2011) does not provide a better fit, even though it was derived for sands with similar age and origin to those considered in this study. Skewness in distributions, mainly at large negative residuals, and trends in residuals mean that errors cannot be explained only by randomness and that functional forms or fitting coefficients must be revised.

6 Proposed correlations for Eastern Canada sands

Several functional forms, including the six previously described equations with non-fixed coefficients, were tested to determine which form best agrees with an independent Eastern Canada seismic piezocone data set. Results of multiple nonlinear regressions show that Eqs. 5, 6, 8, and 9 provide acceptable fits with standard deviations of about 26–30 m/s (see Appendix A). The goodness of fit for the functional form of Hegazy and Mayne (2006) is only slightly better than with the coefficients used in Eq. 7. The standard deviation is 52 m/s and a strong bias is still present in residuals.

It is noteworthy that the lowest standard deviations are always obtained when the effective vertical overburden stress is included in regression instead of depth. As soil unit weights are assumed constant above and below the ground water table (section 4.1.2), this observation simply reflects the effect of the groundwater table depth on the vertical overburden stress profiles.

The choice of I_c as an explanatory variable in a functional form seems natural, at first glance. There is generally a good agreement between soil behaviour types inferred from I_c and soil types defined from grain-size distribution (Jefferies and Davies, 1993; Robertson, 2009) as shown in Figs 3, 4 and 5. However, I_c is an indirect variable computed from the cone tip resistance, the sleeve friction resistance, and the effective overburden pressure, and its incorporation in a functional form can be redundant if one or more of these variables are also part of the equation. Moreover, it is not possible to evaluate the respective contribution of these three variables on the variance associated with I_c in a regression. For these reasons, the sleeve friction resistance is chosen, instead of I_c, as one of the explanatory variables in the regression equation we recommend for Eastern Canada sands. This equation is:

$$V_s = a\, {q_t}^b\, {f_s}^c\, {\sigma'_{v0}}^d \tag{10}$$

where $a = 28.27$, $b = 0.137$, $c = 0.013$, and $d = 0.170$. The three explanatory variables are in kPa and are as previously defined. The standard deviation on Vs is 25 m/s and the confidence intervals for the regression coefficients are, at a 95% confidence level, as follows: 25.17–31.37 for a; 0.120–0.153 for b; 0.002–0.025 for c; and 0.157–0.183 for d. As shown in Fig. 9, the data cloud of predicted versus measured shear wave velocities is now much better aligned with the 1:1 diagonal and residuals are centred around zero. Low and high shear wave velocities are, however, slightly under and overestimated, respectively, the fit being controlled by the high local density of points at intermediate velocities.

Coefficient c in Eq. 10 is low and has a calculated probability p-value greater than those of the other variables (but still significant at a 5% level), which are virtually zero. It means that the sleeve friction resistance has a relatively minor effect in the regression, and that this variable can be dropped without strongly impacting the goodness of fit. We thus propose an alternative regression equation without sleeve friction resistance, and for simplicity, depth in place of the effective vertical overburden stress:

$$V_s = a\, {q_t}^b\, z^c \tag{11}$$

where $a = 39.00$, $b = 0.164$, and $c = 0.137$. Depth z is in m, and other variables are as defined previously. The standard deviation is a little higher at 27 m/s. The confidence intervals at a 95% confidence level are 34.42–43.58, 0.150–0.178, and 0.126–0.149, respectively for coefficients a, b, and c. As with Eq. 10, residuals are much more evenly distributed around zero than for correlations presented in Fig. 8, and the distribution follows approximately a normal curve over the range of residuals (Fig. 9).

The goodness of fit can be evaluated from plots showing residuals, not only as a function of the predicted variable V_s as in Figs 8 and 9, but also as a function of the different explanatory variables for a given regression equation. Fig. 10 shows such plots for the two proposed regression equations 10 and 11. On each plot, residuals are fitted locally with a robust moving average smoothing function (Chambers et al., 1983; NIST, 2012) to help visualize possible patterns or trends in data (solid red line). After a few trials, it was found that a span of 101 data points for the smoothing function gives good results. Larger spans tend to over-smooth data while smaller spans under-smooth data and produce too jagged curves. The two dashed red lines indicate intervals corresponding to two standard deviations calculated as for the mean curves, with a robust moving smoothing function and a span of 101 data points. The marker colours represent the local density of data points (Henson, 2013).

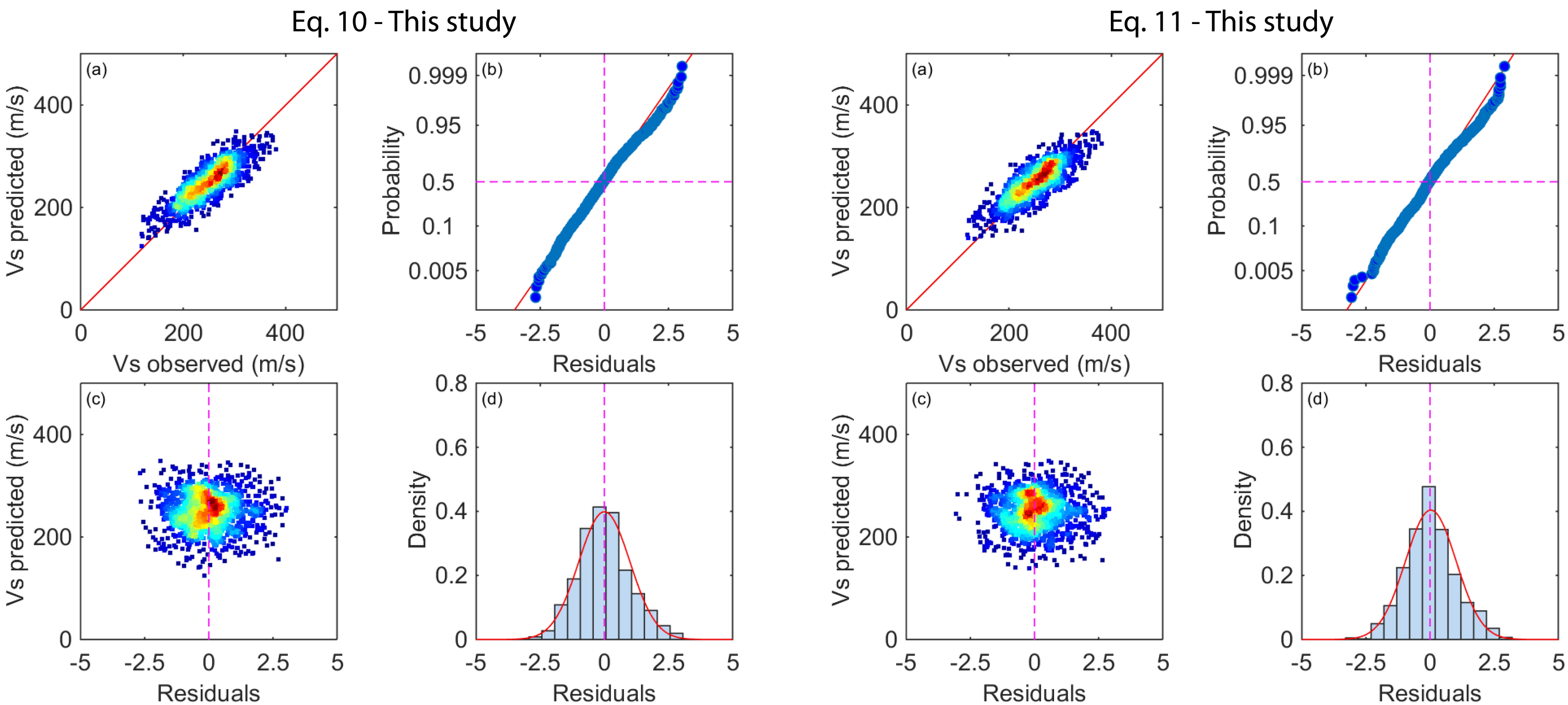

Figure 9 – Plots showing the goodness of fit for the two proposed correlations.

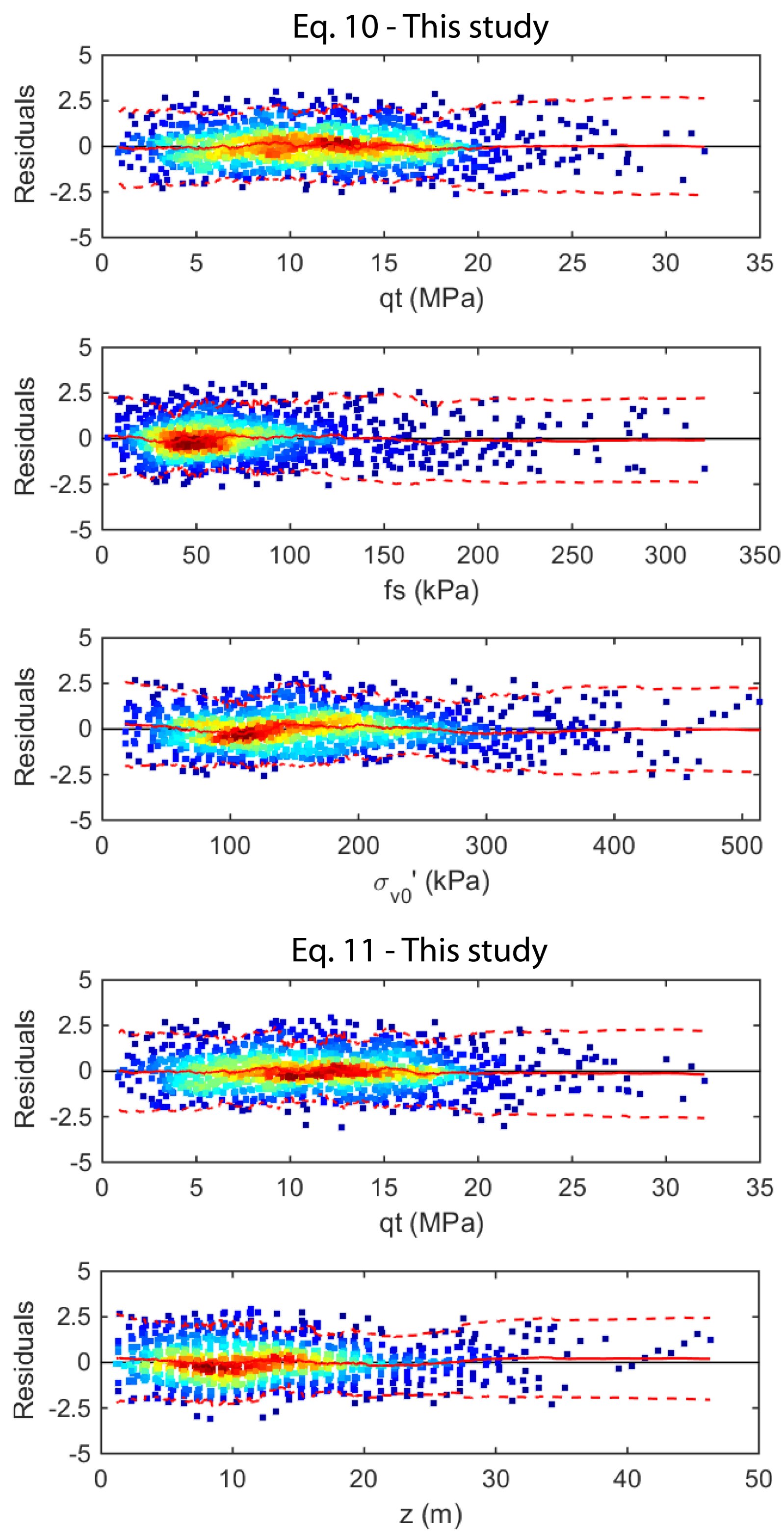

Figure 10 – Variation of residuals with predictor variables for regression equations 10 and 11. Robust moving average curves are in red and dashed red curves correspond to two standard deviations around the moving average curves.

Curves show some waviness, in particular where data points are the densest, but the mean curves remain centred on null residual lines, which is an additional indication that the two proposed regression equations predict reasonably well shear wave velocities. Confidence intervals tend to be slightly wider at large values of the explanatory variables. This increase in variance, due to the much lower number of data points in these data ranges, is, however, sufficiently minor to be ignored for practical applications.

7 Discussions

Even with regression equations 10 and 11 tailored to Eastern Canada cohesionless soils, dispersion around null residual is still important (σ = 25-27 m/s) and a small trend in plots (a) of Fig. 9 is still present. A probable cause of the persistence of a trend is the inadequacy of the functional form of Eqs 10 and 11, and more generally of all the forms tested, which are mainly founded on an empirical basis.

In addition to measurement uncertainties for both Vs and piezocone test parameters, data dispersion can be due to several other factors. Piezocone test profiles were discretized at 1 m depth intervals to correspond with shear wave velocity profiles by calculating the median value of parameters. Considering the median implies that extreme peak values in piezocone test data on these 1 m depth intervals do not significantly influence shear wave velocities, which is a strong implicit, and not verified, assumption. On the other hand, it is also well known that the piezocone test cannot accurately detect thin soil layers with different cone tip resistance or porewater pressure values and that these parameters can be unrepresentative of true values if layers are too thin (Vreugdenhil et al., 1994). Shear wave velocities may thus be more or less correlated to median values depending on soil layering and on the number and magnitude of peak values in an interval.

Another source of uncertainty that may explain dispersion is the age and geological origin of sands. Age is not accounted for in Eqs 10 and 11 as it is not known with the required certainty when sands were deposited during the approximatively 5,000-year time span that extends from late Pleistocene to early Holocene. For the youngest deposits in a given region, the sedimentation environment may have progressively changed in time and space from deltaic to fluvial, or coastal-estuarine conditions with a change in some physical and mechanical properties of sands. The data set may not be as homogeneous as thought and dispersion may also be a consequence of the natural variability of some sand properties that cannot be captured with the functional forms tested in this study involving only piezocone test parameters.

8 Conclusions

Data were compiled from seismic piezocone tests at 107 sites located along the St. Lawrence River and its tributaries in Eastern Canada. The data set was filtered to retain only sands by applying thresholds on the normalized soil behaviour type index I_c and normalized porewater pressure ratio B_q. Shear wave velocity was computed from piezocone test parameters using six regression equations commonly used in practice. Results were compared to observed shear wave velocities calculated from seismic piezocone test recordings. It is shown that these six equations predict shear wave velocities with a significant bias. As a result, two new equations specifically developed for Eastern Canada sands are proposed. They allow the estimation of shear wave velocities with a standard deviation of 25-27 m/s, which is deemed acceptable for detecting anomalous measured values, for regional seismic zonation, or for seismic site classification in low risk projects.

Acknowledgements

This study was supported by the Public Safety Geoscience Program, Earth Science Sector, Natural Resources Canada, and represents ESS Contribution 2016-30717. The authors would like to thank the Ministère des Transports, de la Mobilité Durable et de l'Électrification des Transports du Québec, and Englobe Corp., for the permission to use and present geotechnical data. The authors also wish to thank Heather Crow and Denis Demers for their review of an early draft of this report.

References

[1] Andrus, R.D., Stokoe, K.H. and Juang, C.H. 2004. Guide for shear-wave-based liquefaction potential evaluation. Earthquake Spectra, 20(2): 285–308.

[2] Andrus, R.D., Mohanan, N.P., Piratheepan, P., Ellis, B.S. and Holzer, T.L. 2007. Predicting shear-wave velocity from cone penetration resistance. Proceedings, 4th International Conference on Earthquake Engineering, Thessaloniki, Greece, Paper No. 1454.

[3] ASTM, 2012. Standard test method for electronic friction cone and piezocone penetration testing of soils. Standard D5778-12, ASTM International, West Conshohocken, PA, 2012, DOI: 10.1520/D5778-12, www.astm.org.

[4] Baldi, G., Belloti, R., Ghionna, V., Jamiolkowski, M. and Lo Presti, D. 1989. Modulus of sands from CPTs and DMTs. Proceedings, 12th International Conference on Soil Mechanics and Foundation Engineering, Rio de Janeiro, Brazil, Vol. 1, 165-–170.

[5] Boulanger, R.W and Idriss, I.M. 2006. Liquefaction susceptibility criteria for silts and clays. Journal of Geotechnical and Geoenvironmental Engineering, ASCE, 132(11):1413–1426.

[6] Boulanger, R.W and Idriss, I.M. 2016. CPT-based liquefaction triggering procedure. Journal of Geotechnical and Geoenvironmental Engineering, ASCE, 142(2), DOI: 10.1061/(ASCE)GT.1943-5606.0001388.

[7] Clayton, C.R.I. 2011. Stiffness at small strain: research and practice. Géotechnique, 61(1):5–37.

[8] Cunning, J.C., Robertson, P.K. and Sego, D.C. 1995. Shear wave velocity to evaluate in situ state of cohesionless soils. Canadian Geotechnical Journal, 32:848–858.

[9] Dobry, R. and Abdoun, T. 2015. Third Ishihara Lecture: An investigation into why liquefaction charts work: A necessary step toward integrating the states of art and practice. Soil Dynamics and Earthquake Engineering, 68:40-56.

[10] Chambers, J.M., Cleveland, W.S., Kleiner, B. and Tukey, P.A. 1983. Graphical methods for data analysis. Wadsworth & Brooks/Cole Statistics/Probability Series, 408p.

[11] Eilers, P.H.C and Goeman, J.J. 2004. Enhancing scatterplots with smoothed densities. Bioinformatics, 20:623–628.

[12] Hegazy, Y.A. and Mayne, P.W. 1995. Statistical correlations between V_s and cone penetration data for different soil type. Proceedings, International Symposium on Cone Penetration Testing, CPT'95, Linköping, Sweden, Vol. 2, 173–178.

[13] Hegazy, Y.A. and Mayne, P.W. 2006. A global statistical correlation between shear wave velocity and cone penetration data. Proceedings, GeoShangai, Site and Geomaterial Characterization, ASCE GSP-149, 243–248.

[14] Henson, R. 2013. Function *dscatter* — Flow cytometry data reader and visualization. Matlab® Central File Exchange, retrieved Nov. 14, 2014.

[15] Houlsby, G.T. and Wroth, C.P. 1989. The influence of soil stiffness and lateral stress on the results of in-situ soil tests. Proceedings, 12th International Conference on Soil Mechanics and Foundation Engineering, Rio de Janeiro, Brazil, Vol. 1, 227–232.

[16] Hunter, J.A. and Crow, H.L. 2012. Shear wave velocity measurement guidelines for Canadian seismic site characterization in soil and rock. J.A. Hunter and H.L. Crow (eds.), Open File 7078, Geological Survey of Canada, 227p.

[17] Jefferies, M.G. and Davies, M.P. 1993. Use of CPTU to estimate equivalent SPT N60. Geotechnical Testing Journal, 16(4):458–468.

[18] Karray, M., Lefebvre, G., Ethier, Y. and Bigras, A. 2011. Influence of particle size on the correlation between shear wave velocity and cone tip resistance. Canadian Geotechnical Journal, 48:599–615.

[19] Kim, D.S., Bang, E.S. and Kim, W.C. 2005. Evaluation of various downhole data reduction methods for obtaining reliable Vs profiles. Geotechnical Testing Journal, 27(6):1–13.

[20] Lunne, T., Robertson, P.K. and Powell, J.J.M. 1997. Cone penetration testing in geotechnical engineering, Spon Press, 312p.

[21] McGann, C.R., Bradley, B.A., Taylor, M.L., Wotherspoon, L.M. and Cubrinovski, M. 2015a. Applicability of existing empirical shear wave velocity correlations to seismic cone penetration test data in Christchurch New Zealand. Soil Dynamics and Earthquake Engineering, 75:76–86.

[22] McGann, C.R., Bradley, B.A., Taylor, M.L., Wotherspoon, L.M. and Cubrinovski, M. 2015b. Development of empirical correlation for predicting shear wave velocity of Christchurch soils from cone penetration test data. Soil Dynamics and Earthquake Engineering, 75:66–75.

[23] Mayne, P.W. 2007. Cone penetration testing — A synthesis of highway practice. NHCRP Synthesis 368, 126p.

[24] NIST, 2012. Engineering statistics — e-Handbook of statistical methods. National Institute of Standards and Technology, `www.itl.nist.gov/div898/handbook`, last consulted on 2016/05/02.

[25] Perret, D., Charrois, E. and Bolduc, M. 2016. Shear wave velocity estimation from piezocone test data for Eastern Canada sands. Proceedings, 69th Canadian Geotechnical Conference, Vancouver, Canada, 9p.

[26] Petrakis, E. and Dobry, R. 1987. Micromechanical modelling of granular soil at small strain by arrays of elastic spheres. Journal of Geotechnical and Geoenvironmental Engineering, ASCE, 195(GT7):871–880.

[27] Puppala, A.J., Acar, Y.B. and Tumay, M.T. 1995. Cone penetration in very weakly cemented sands. Journal of Geotechnical and Geoenvironmental Engineering, ASCE, 121(8):589–600.

[28] Robertson, P.K. 2009. Interpretation of cone penetration tests — a unified approach. Canadian Geotechnical Journal, 46:1337–1355.

[29] Robertson, P.K. and Cabal, K.L. 2015. Guide to cone penetration testing for geotechnical engineering. Gregg Drilling & Testing, Inc., 6th Edition, 143p.

[30] Salgado, R., Mitchell, J.K. and Jamiolkowski, M. 1997. Cavity expansion and penetration resistance in sand. Journal of Geotechnical and Geoenvironmental Engineering, ASCE, 123(4):344–354.

[31] Salgado, R. 2014. Experimental research on cone penetration resistance. Geo-Congress, ASCE, GSP-235, 140–163.

[32] Santamarina, J.C. and Cascante, G. 1996. Stress anisotropy and wave propagation: a micromechanical view. Canadian Geotechnical Journal, 33:770–782.

[33] Schafer, R.W. 2011. What is a Savitzky-Golay filter? IEEE Signal Processing Magazine, 111, DOI: 10.1109/MSP.2011.941097.

[34] Schnaid, F. 2005. Geo-characterization and properties of natural soils by in situ tests. Proceedings, 15th International Conference on Soil Mechanics and Foundation Engineering, Osaka, Japan, Vol. 1, 3–45.

[35] Schnaid, F. and Yu, H.S. 2007. Interpretation of the seismic cone test in granular soils. Géotechnique, 57(3):265–272.

[36] Vreugdenhil, R., Davis, R. and Berrill, J. 1994. Interpretation of cone penetration results in multilayered soils. International Journal of Numerical and Analytical Methods in Geomechanics, 18:585–599.

[37] Wair, B.R., DeJong, J.T. and Shantz, T. 2012. Guidelines for estimation of shear wave velocity profiles. Report PEER 2012/08, Pacific Earthquake Engineering Research Center, 95p.

Appendix A Additional figures for some tested regression equations

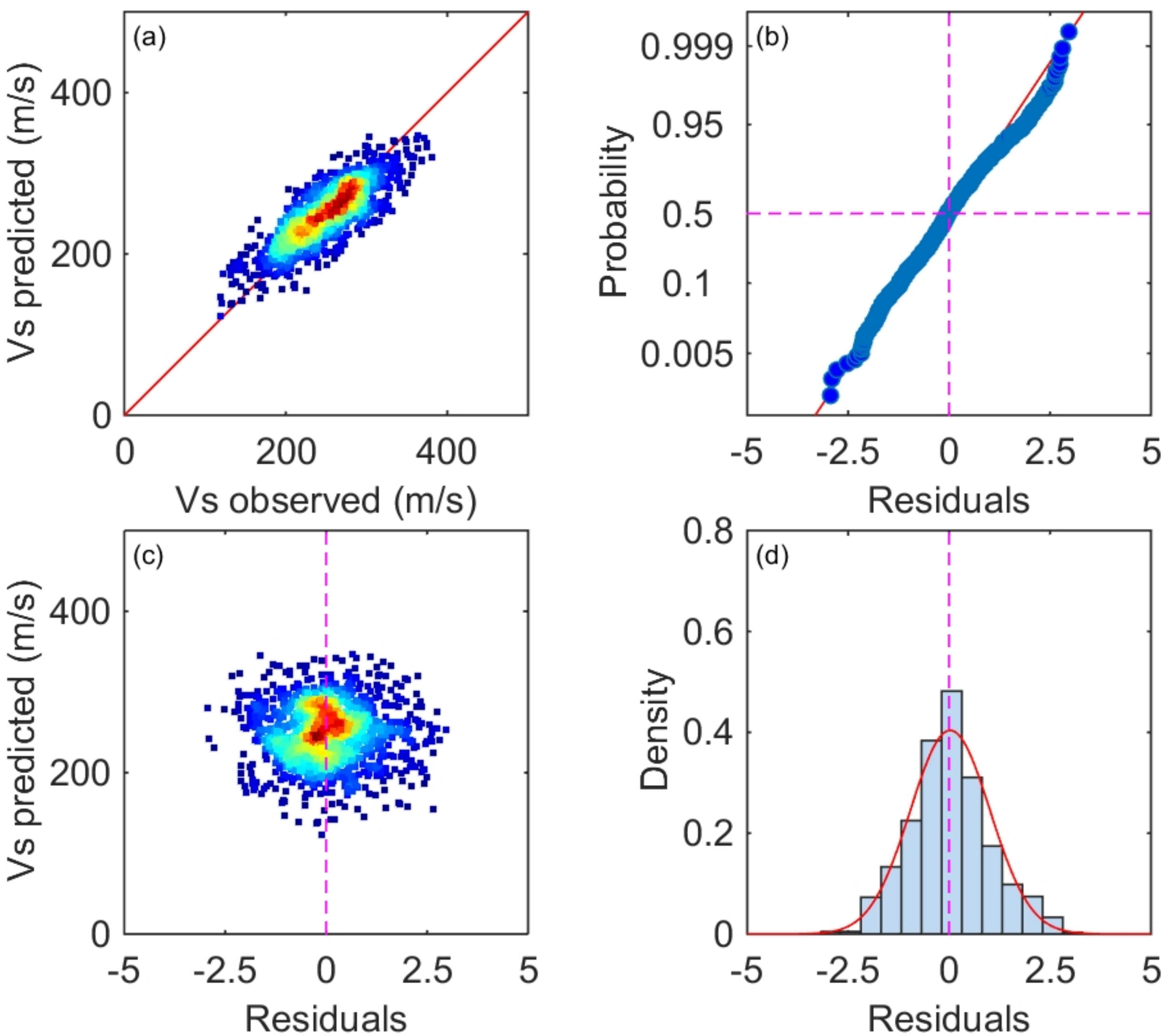

Figure A.1 – Plots showing the goodness of fit for the Andrus et al. (2007) regression equation with free fit parameters (see Eq. 5). The new equation with free fit parameters is:
$V_s = 28.03\ q_t^{0.194}\ I_c^{0.136}\ z^{0.123}$, with a standard deviation $\sigma = 26$ m/s.

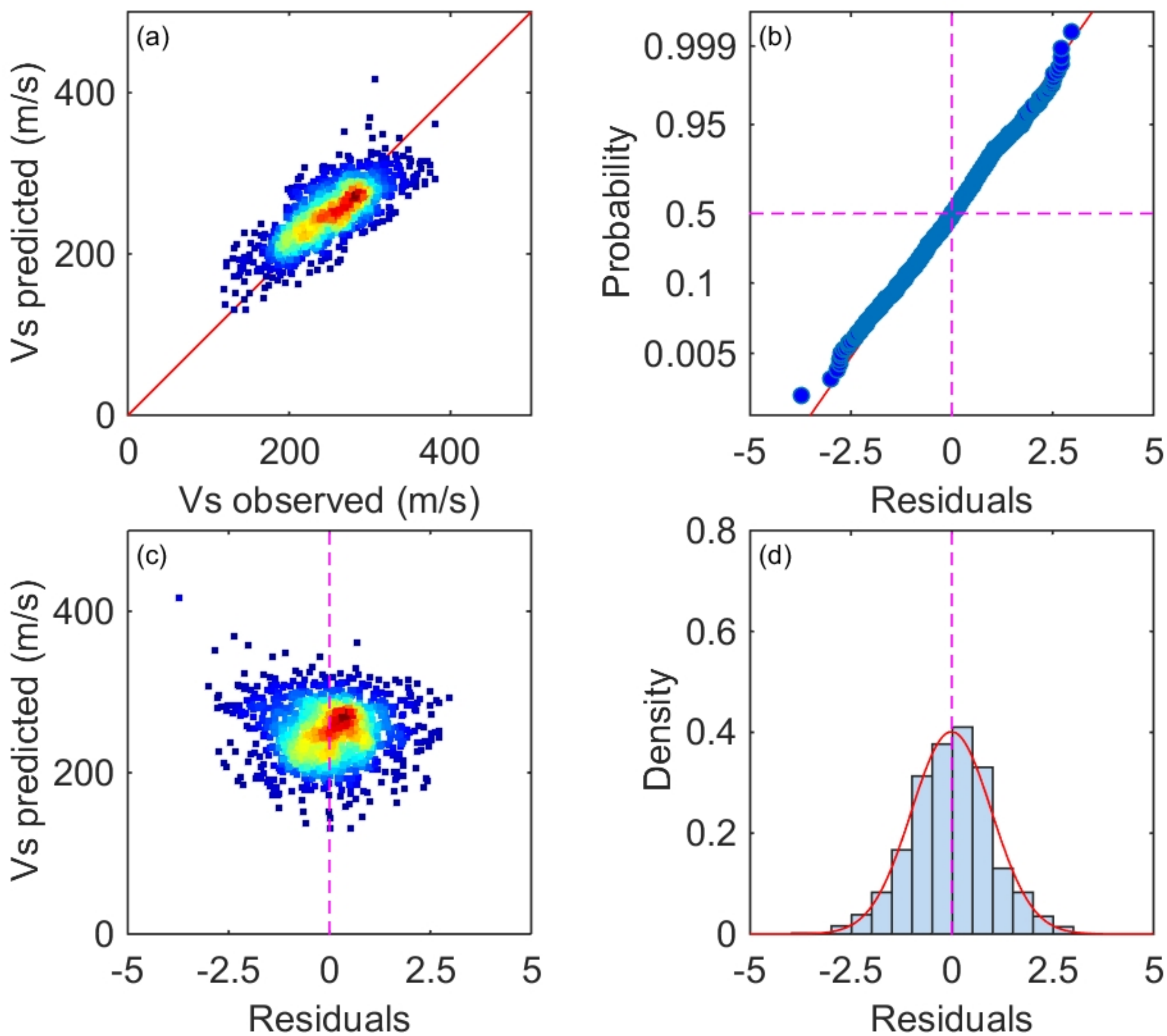

Figure A.2 – Plots showing the goodness of fit for the Robertson (2009) regression equation with free fit parameters (see Eq. 6). The new equation with free fit parameters is $V_s = \left[10^{\,(0.405\ I_c\,+\,4.406)}\ \frac{q_t - \sigma_{v0}}{p_a}\right]^{0.333}$, with a standard deviation σ = 30 m/s.

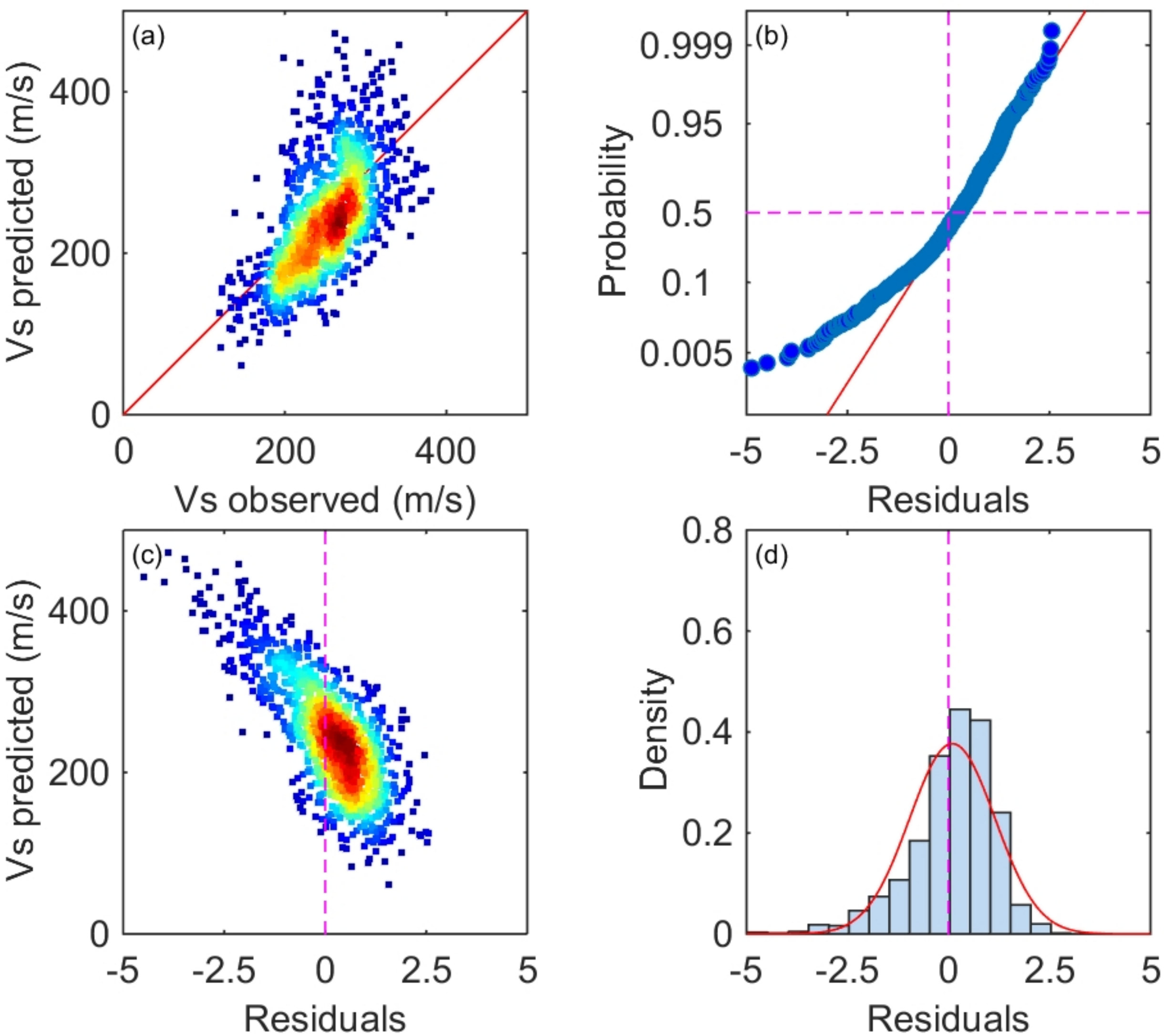

Figure A.3 – Plots showing the goodness of fit for the Hegazy and Mayne (2006) regression equation with free fit parameters (see Eq. 7). The new equation with free fit parameters is $V_s = 0.196\, q_{c1N} \left(\frac{\sigma'_{v0}}{p_a}\right)^{1.393} e^{0.377\, I_c}$, with a standard deviation $\sigma = 52$ m/s.

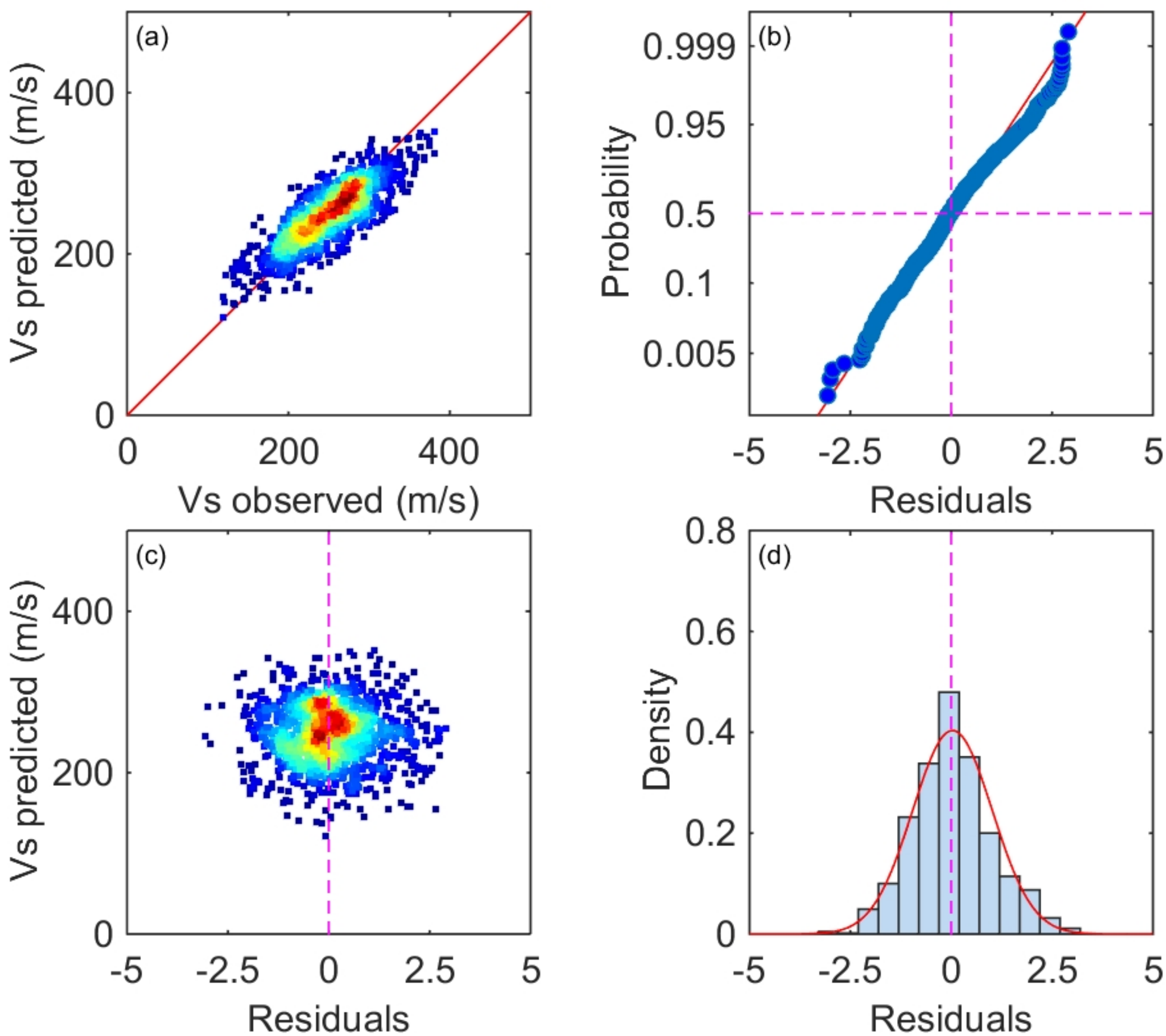

Figure A.4 – Plots showing the goodness of fit for the McGann et al. (2015b) regression equation with free fit parameters (see Eq. 8). The new equation with free fit parameters is $V_s = 39.14\ q_c{}^{0.164}\ f_s{}^{0.001}\ z^{0.138}$, with a standard deviation σ = 27 m/s.

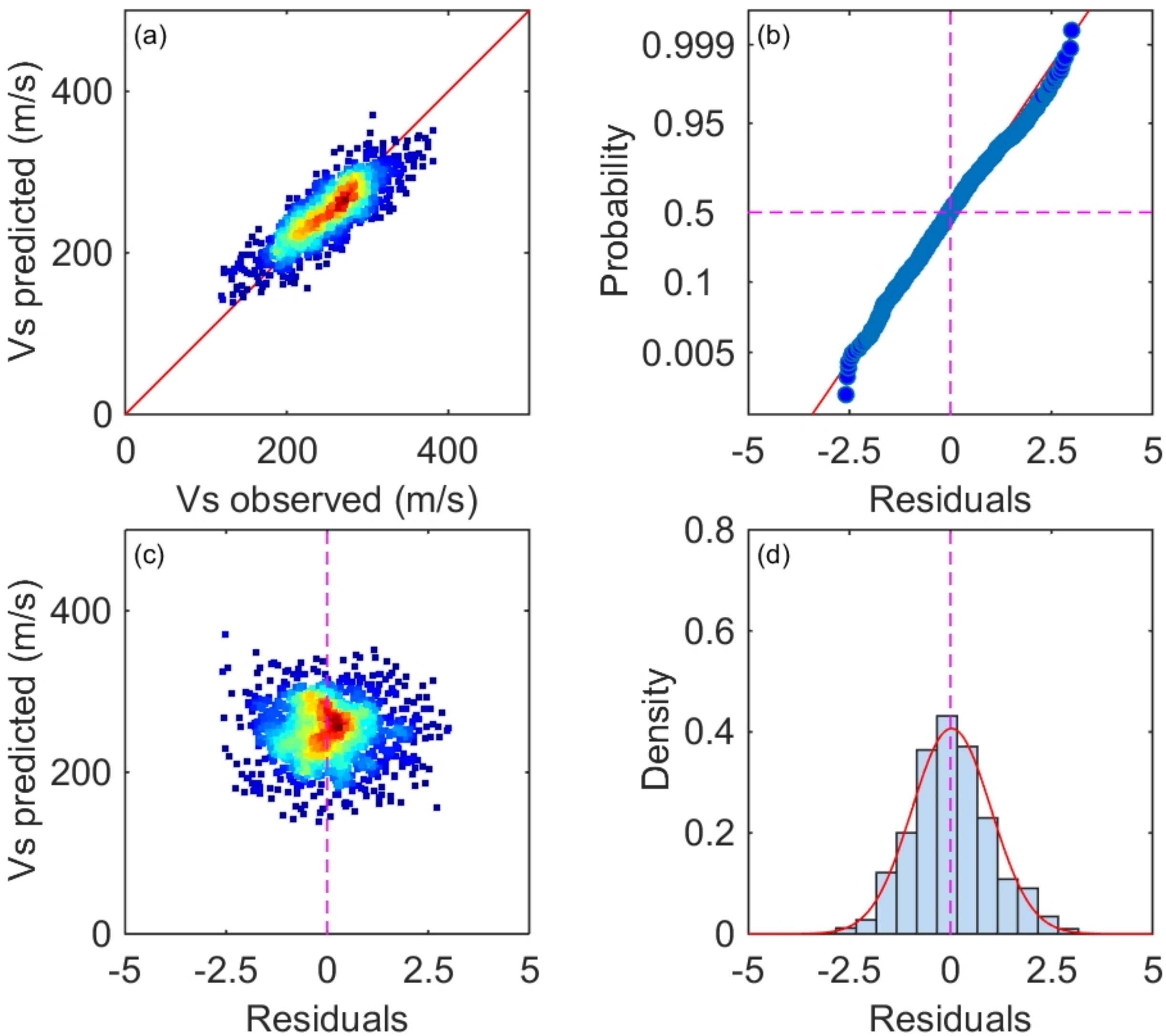

Figure A.5 – Plots showing the goodness of fit for the Karray et al. (2011) regression equation with free fit parameters (see Eq. 9). The new equation with free fit parameters is $V_s = 46.76\ {q_{c1}}^{0.167}\ {I_c}^{0.088} \left(\frac{\sigma'_{v0}}{p_a}\right)^{0.242}$, with a standard deviation $\sigma = 26$ m/s.

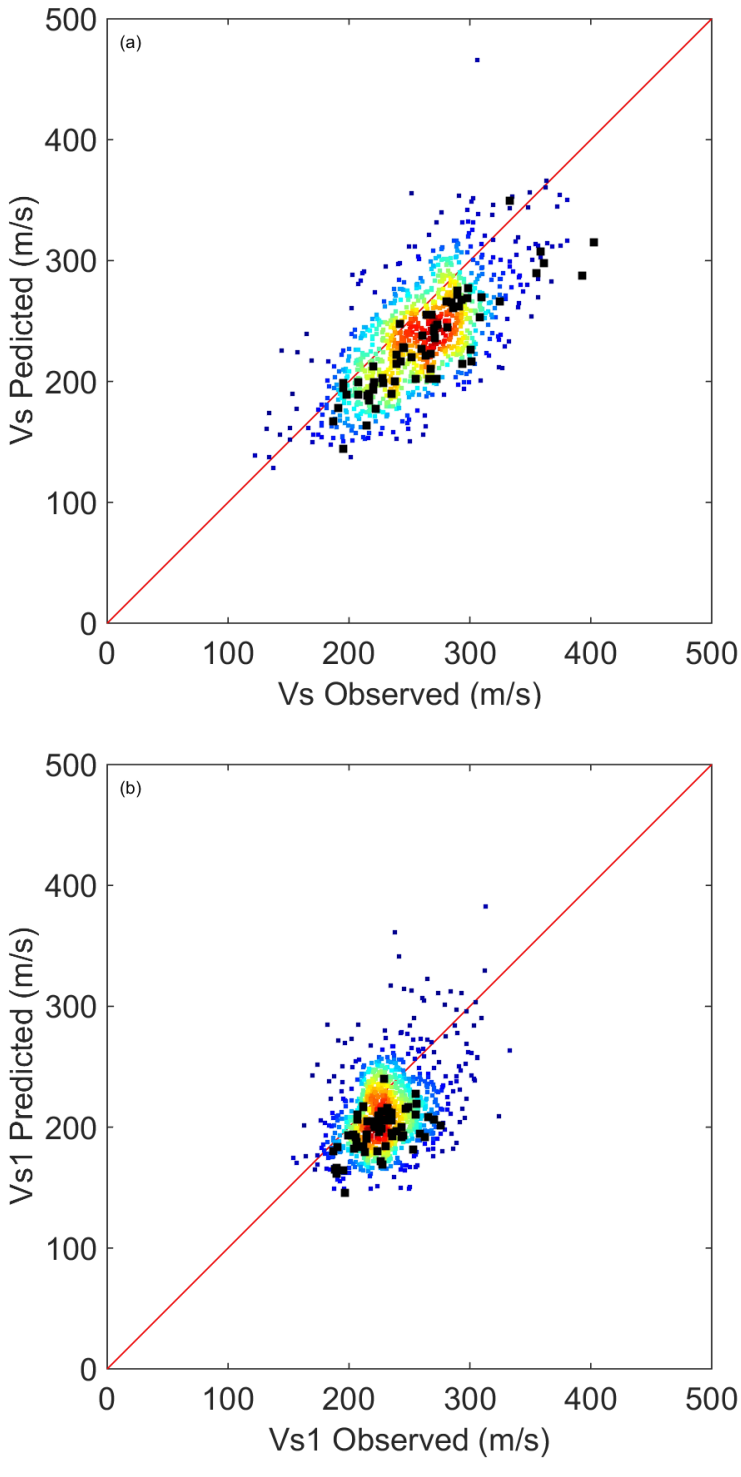

Figure A.6 – Plots showing the goodness of fit for the Karray et al. (2011) regression equation, (a) in terms of V_s (see Eq. 9), and (b), in terms of the normalized parameter V_{s1}. Filled black squares show values calculated directly from the median grain-size D_{50} (see Eq. 15 in Karray et al., 2011) for soil samples retrieved at a few seismic piezocone test sites. Using D_{50} instead of I_c does not improve the goodness of fit.

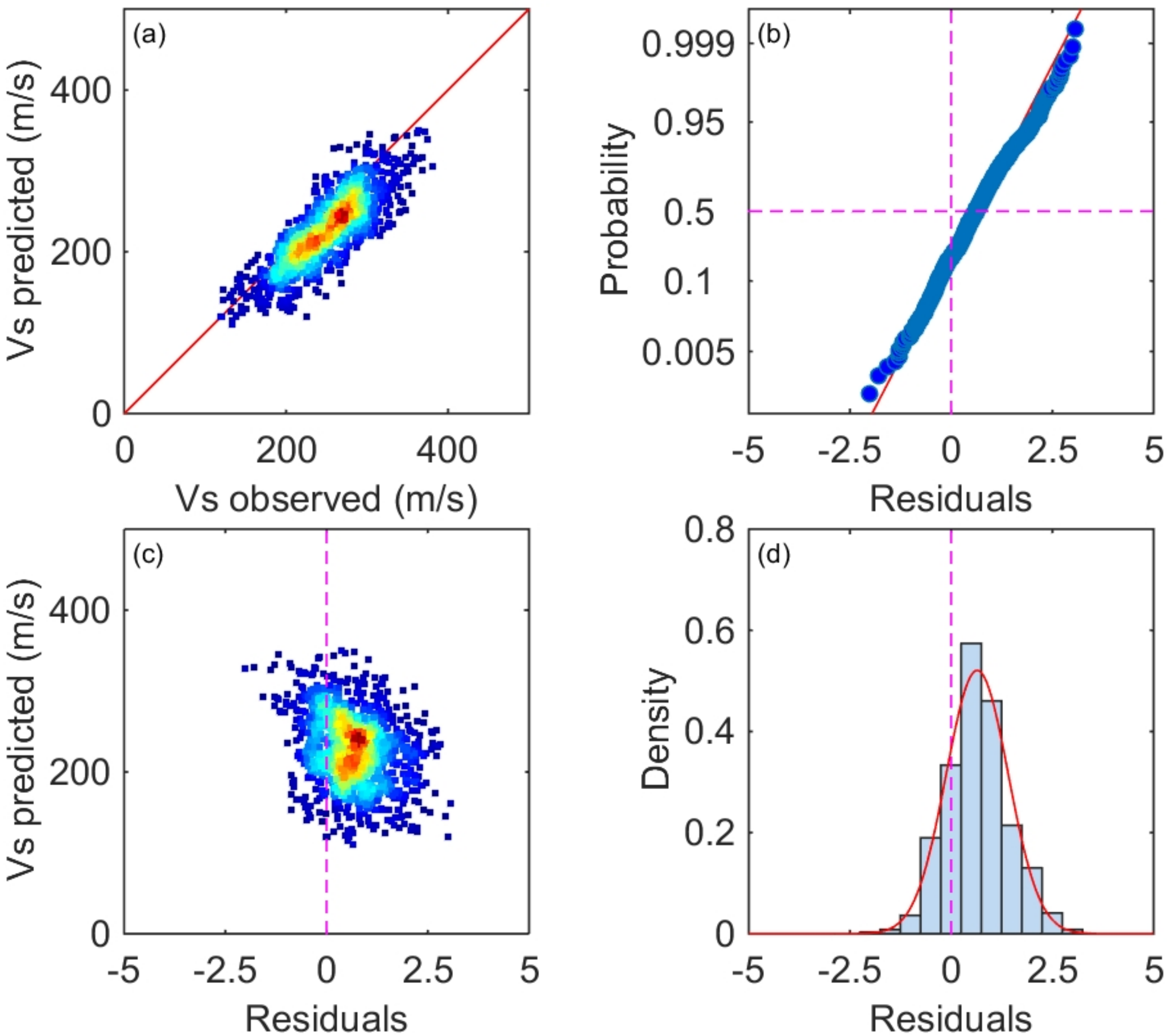

Figure A.7 – Plots showing the goodness of fit for the Baldi et al. (1989) regression equation (Eq. A.7): $V_s = 277\ {q_c}^{0.13}\ {\sigma'_{v0}}^{0.27}$ with q_c and σ'_{v0} in MPa.

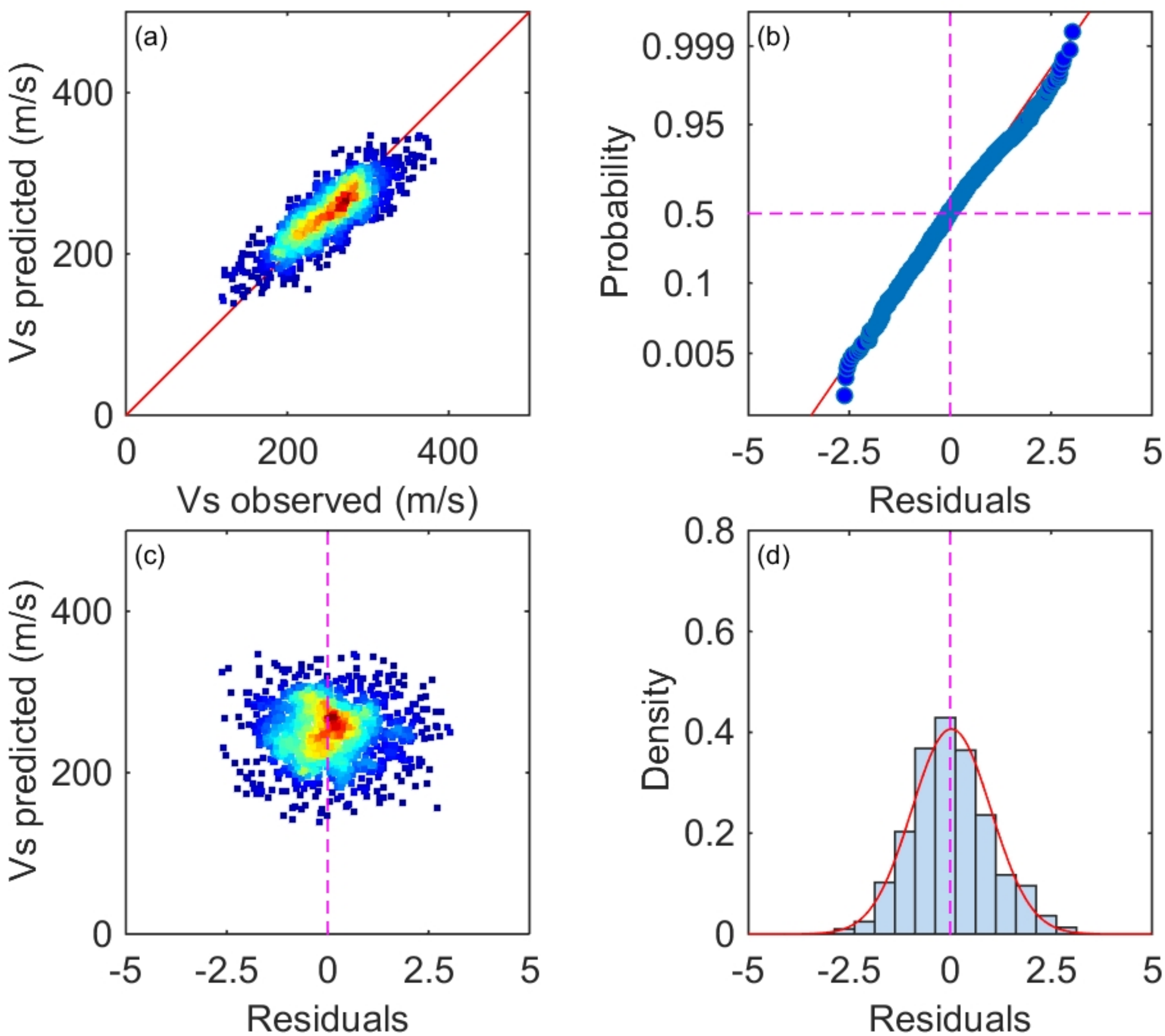

Figure A.8 – Plots showing the goodness of fit for the Baldi et al. (1989) regression equation with free fit parameters (see Eq. A.7). The new equation with free fit parameters is $V_s = 238.06\ q_c{}^{0.150}\ \sigma'_{v0}{}^{0.165}$ with q_c and σ'_{v0} in MPa. The standard deviation is $\sigma = 26$ m/s.

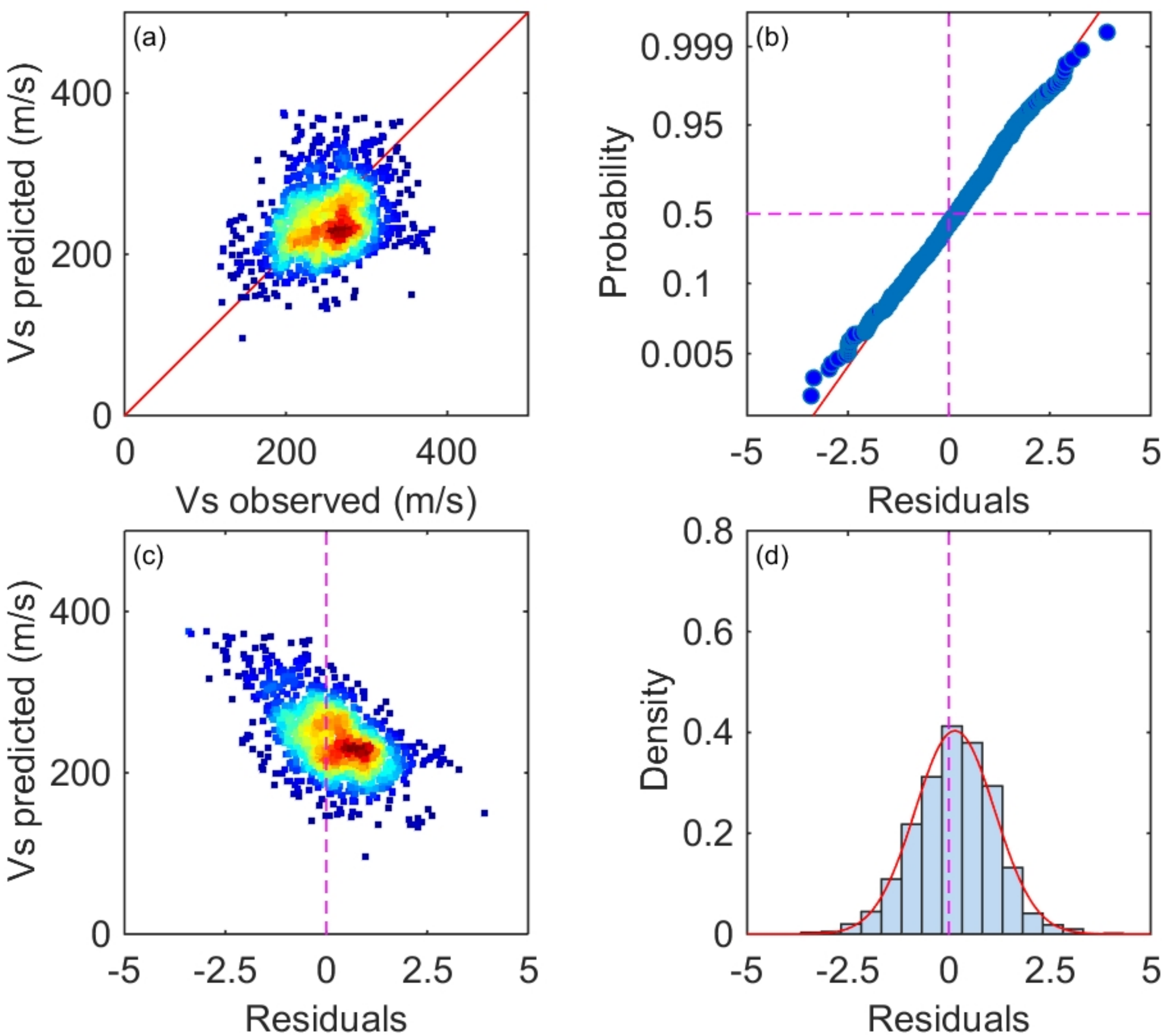

Figure A.9 – Plots showing the goodness of fit for the Hegazy and Mayne (1995) regression equation (Eq. A.9): $V_s = \left(10.1\ \log_{10} q_t\ -\ 11.4\right)^{1.67} \left(100\ \frac{f_s}{q_t}\right)^{0.3}$ with q_t and f_s in kPa.

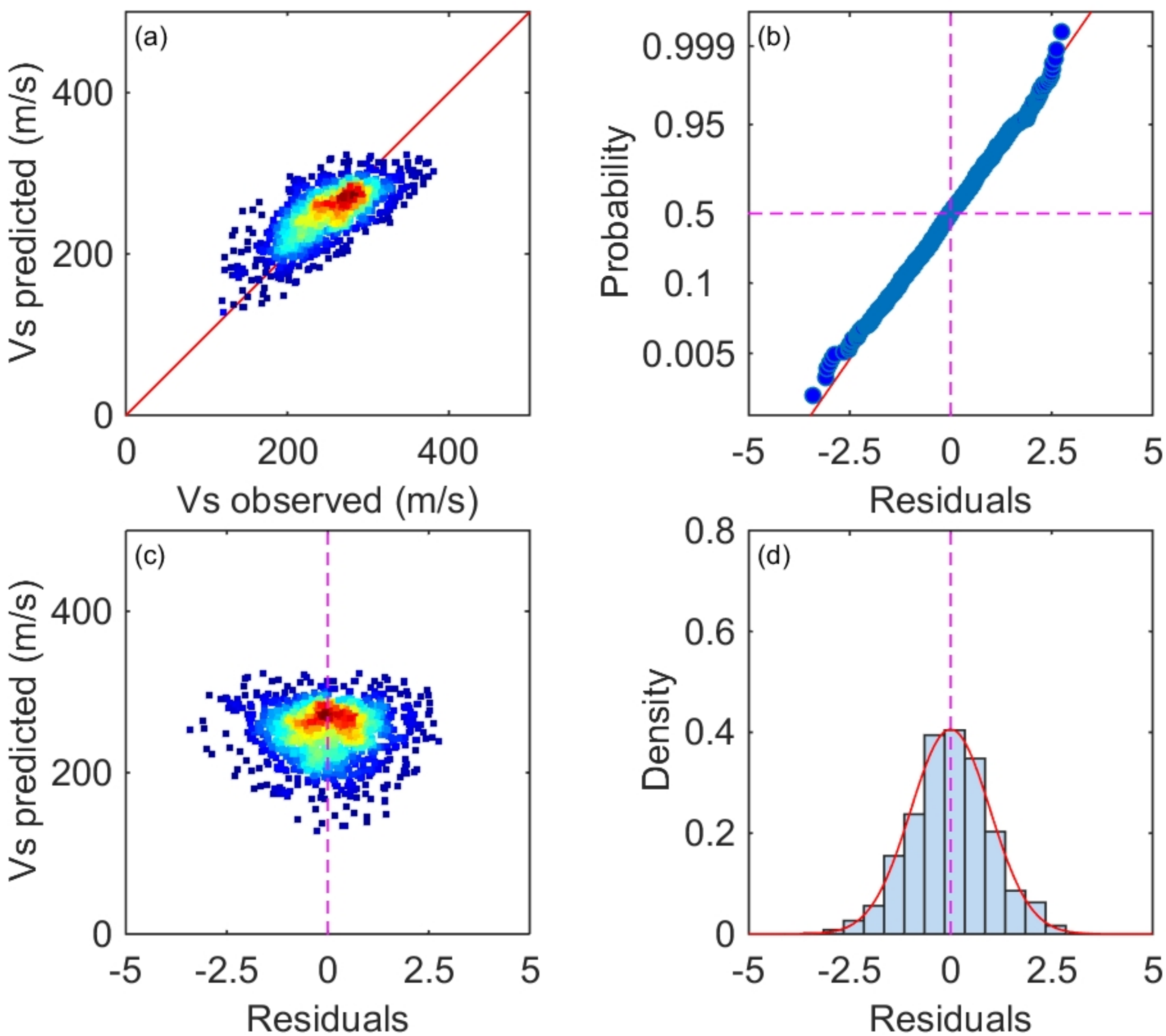

Figure A.10 – Plots showing the goodness of fit for the Hegazy and Mayne (1995) regression equation with free fit parameters (see Eq. A.9): $V_s = \left(1.687\ \log_{10} q_t\ +\ 1.063\right)^{2.673} \left(100\ \frac{f_s}{q_t}\right)^{-0.019}$ with q_t and f_s in kPa. The standard deviation is σ = 32 m/s.

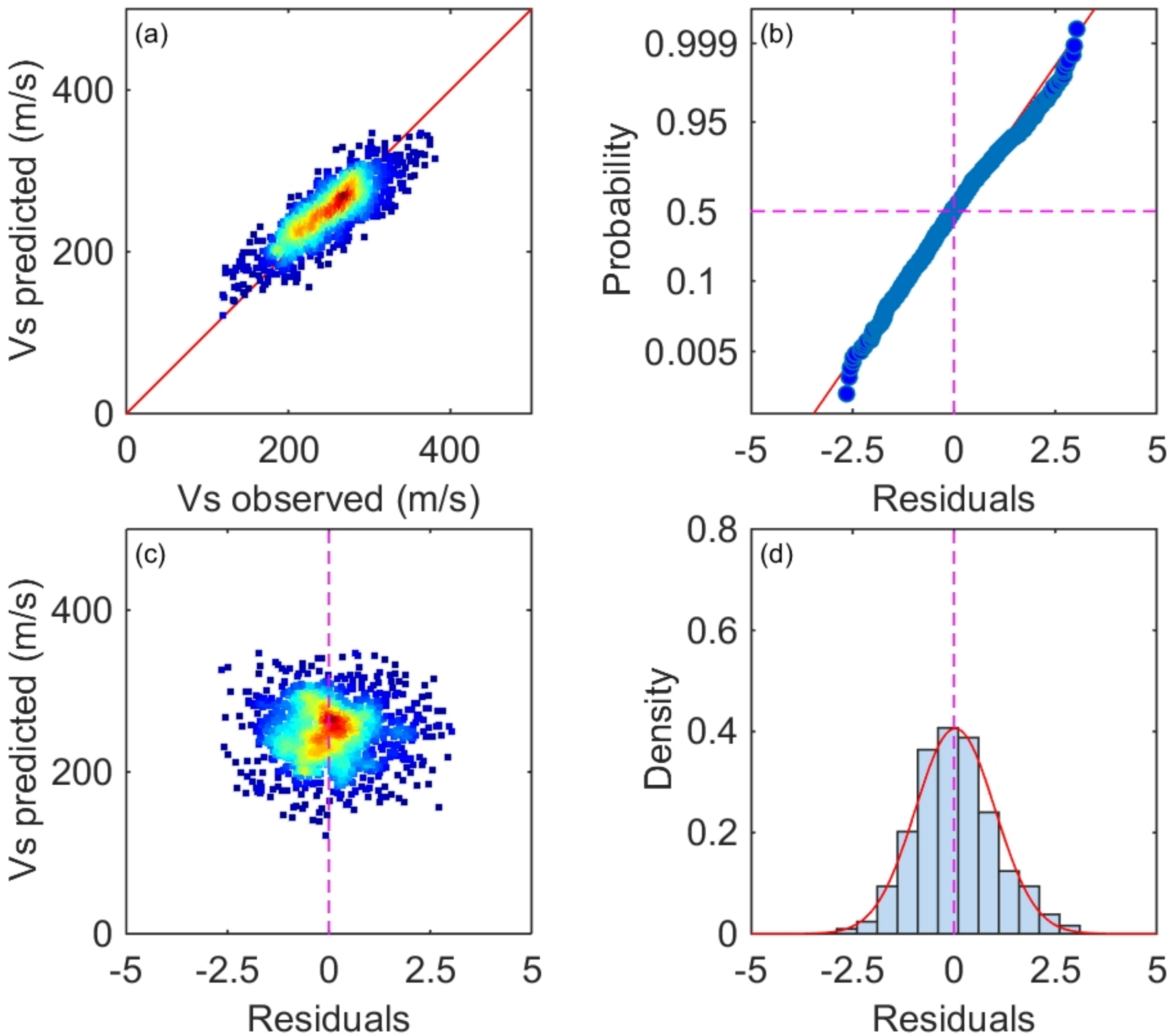

Figure A.11 – Plots showing the goodness of fit for the following regression equation (Eq. A.11): $V_s = 27.57\ {q_t}^{0.073}\ I_c^{0.073}\ {\sigma'_{v0}}^{0.167}$ with q_t and σ'_{v0} in kPa. The standard deviation is $\sigma = 26$ m/s.

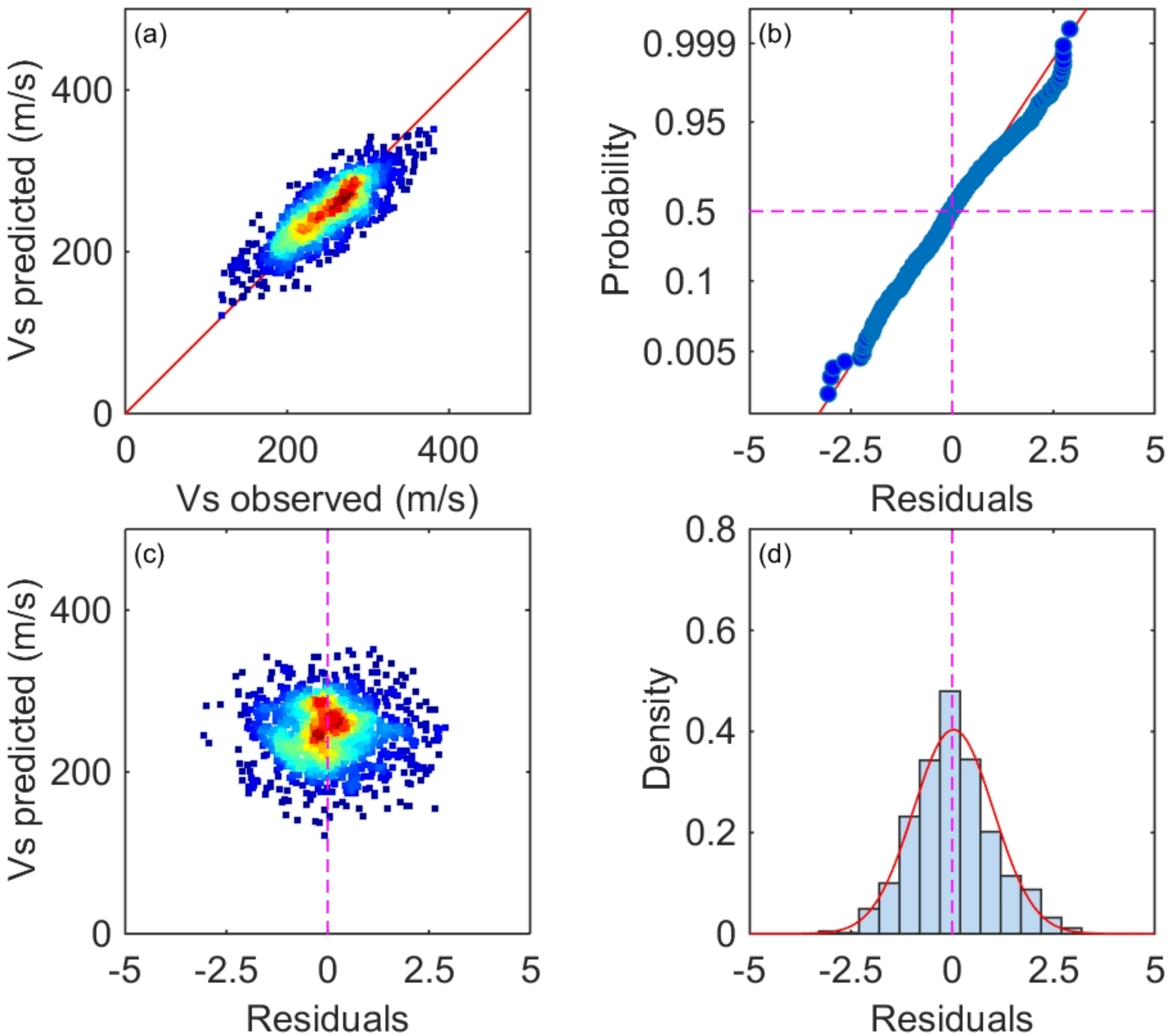

Figure A.12 – Plots showing the goodness of fit for the following regression equation (Eq. A.12): $V_s = 39.14\ q_c^{0.163}\ z^{0.138}$ with q_c in kPa. The standard deviation is σ = 27 m/s.

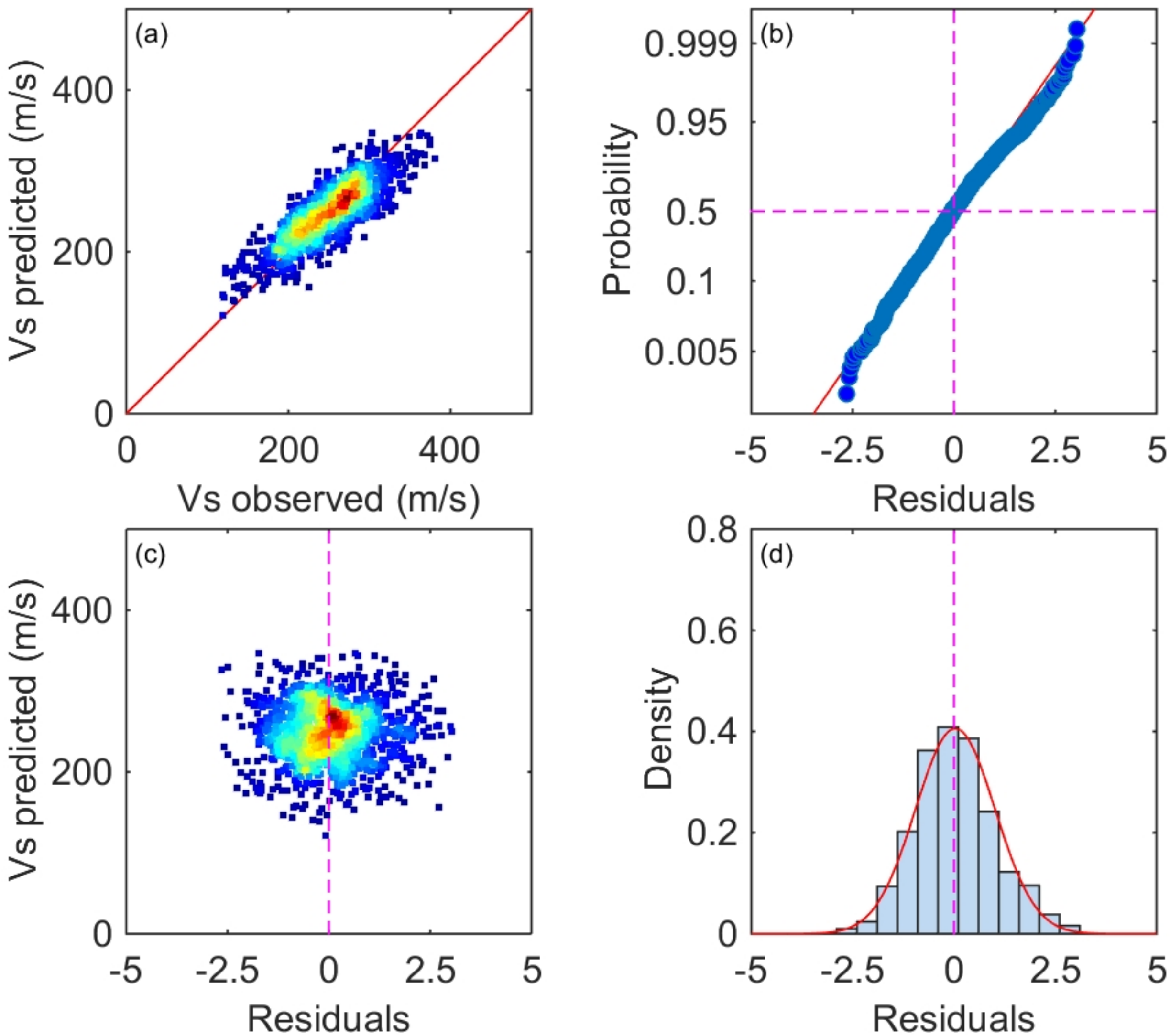

Figure A.13 – Plots showing the goodness of fit for the following regression equation (Eq. A.13): $V_s = 27.570\ q_t^{0.147} {\sigma'_{v0}}^{0.167}$ with q_t and σ'_{v0} in kPa. The standard deviation is $\sigma = 25$ m/s.

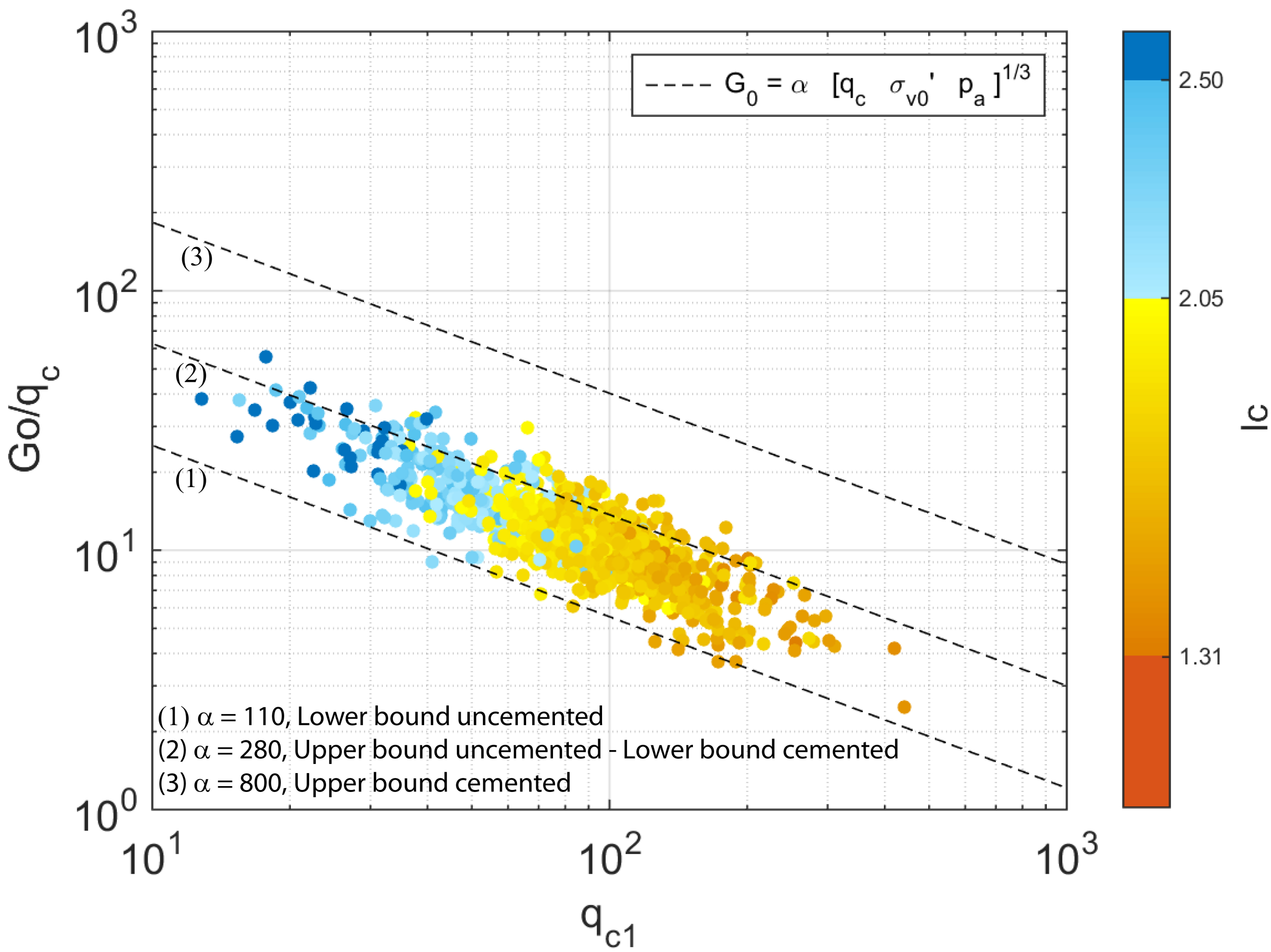

Figure A.14 – Relationship between $\frac{G_0}{q_c}$ and q_{c1} according to Fig. 44 and Eq. 65 in Schnaid (2005). The I_c scale on the right extends from 1.00 to 2.60.

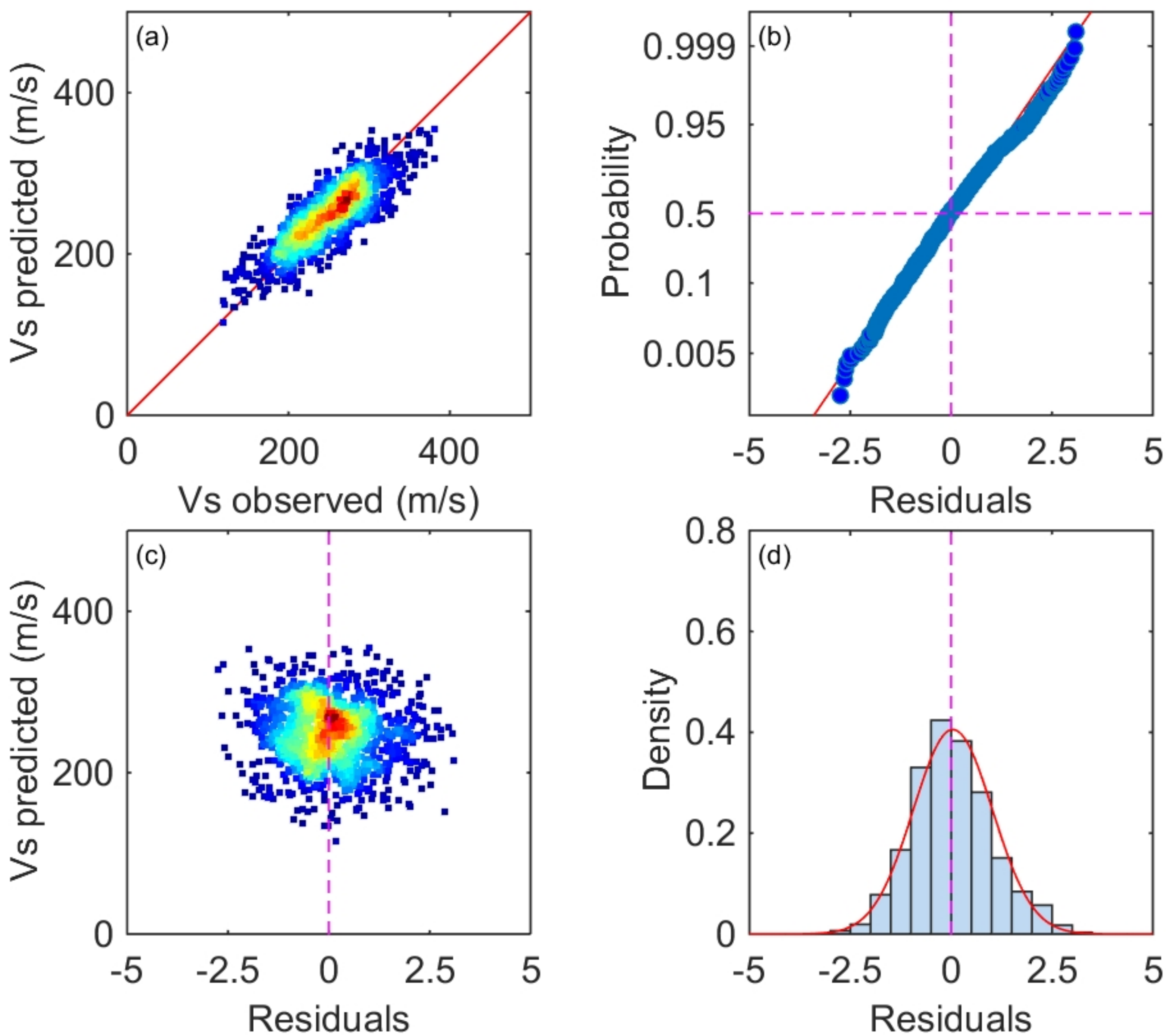

Figure A.15 – Plots showing the goodness of fit in terms of V_s for the Schnaid (2005) regression functional form (Eq. A.15): $G_0 = \alpha \sqrt[3]{q_c \, \sigma'_{v0} \, p_a}$, with q_c, σ'_{v0}, and p_a in kPa. The best fit parameter is $\alpha = 220$ and the standard deviation is $\sigma = 26$ m/s.

Appendix B   Seismic piezocone test data

The seismic piezocone test data set used in this study is provided in spreadsheet files, one for each site investigated. Files are numbered consecutively, from 001.xls to 107.xls, without following a specific order in terms of geographic location. The first data sheet (*CPTu Profiles*) of a given file presents data for the following parameters: the depth z in meter, the raw cone tip resistance q_c in MPa, the sleeve friction resistance f_s in kPa, the porewater pressure u_2 in kPa, and the corrected cone tip resistance q_t in MPa. Shear wave velocities V_s, in m/s, are provided in the second data sheet (*Vs Profile*) as a function of depth.